January 2002 • NREL/SR-520-31458

Subcontractor Report

Device Physics of Thin-Film Polycrystalline Cells and Modules

Final Report
February 1998—August 2001

J. R. Sites
Colorado State University
Fort Collins, Colorado

National Renewable Energy Laboratory

1617 Cole Boulevard
Golden, Colorado 80401-3393

NREL is a U.S. Department of Energy Laboratory
Operated by Midwest Research Institute • Battelle • Bechtel

Contract No. DE-AC36-99-GO10337

January 2002 • NREL/SR-520-31458

Device Physics of Thin-Film Polycrystalline Cells and Modules

Final Report
February 1998—August 2001

J. R. Sites
Colorado State University
Fort Collins, Colorado

NREL Technical Monitor: B. von Roedern

Prepared under Subcontract No. XAK-8-17619-07

National Renewable Energy Laboratory

1617 Cole Boulevard
Golden, Colorado 80401-3393

NREL is a U.S. Department of Energy Laboratory
Operated by Midwest Research Institute • Battelle • Bechtel

Contract No. DE-AC36-99-GO10337

NOTICE

Available electronically at http://www.osti.gov/bridge

Available for a processing fee to U.S. Department of Energy
and its contractors, in paper, from:

U.S. Department of Energy
Office of Scientific and Technical Information
P.O. Box 62
Oak Ridge, TN 37831-0062
phone: 865.576.8401
fax: 865.576.5728
email: reports@adonis.osti.gov

Available for sale to the public, in paper, from:

U.S. Department of Commerce
National Technical Information Service
5285 Port Royal Road
Springfield, VA 22161
phone: 800.553.6847
fax: 703.605.6900
email: orders@ntis.fedworld.gov
online ordering: http://www.ntis.gov/ordering.htm

Printed on paper containing at least 50% wastepaper, including 20% postconsumer waste

SUMMARY

Work has been performed at Colorado State University on basic measurements of CdTe and CI(G)S solar cells fabricated at a number of collaborating laboratories. The first area of emphasis has been to quantitatively deduce the loss mechanisms in these cells, and to make appropriate comparisons that illuminate where progress in being made. Cells evaluated include those at or near record efficiencies and those made with new processing strategies.

A second area of emphasis, the role of impurities, has focused on sodium in CIS. Cells made with varying amounts of sodium added during CIS deposition were fabricated at NREL using four types of substrates. Best performance was achieved with 0.01 to 0.1 at.% sodium.

The third area of study has been small-spot measurement of micro-nonuniformities. A new facility was built to focus a laser beam onto a solar cell with 1-μm beam size, 1-μm resolution and repeatability, and one-sun intensity. Specific projects to date have focused on CdTe and have included the local effect of $CdCl_2$, local intermixing of sulfur, and the effect of temperature-induced stress.

Documentation of cell changes at elevated temperatures has been the fourth area of study. Changes seen in CdTe J-V curves are almost certainly related to diffusion of copper from the back contact, but in most cases an activation-energy model predicts sufficient stability for a 30-year product lifetime. Transients seen in some CIS cells are primarily seen in fill-factor and are primarily driven by voltage bias rather than illumination condition.

The final area of emphasis has been numerical simulations of CdTe and CI(G)S cells. Results with CdTe are able to replicate experimental data, have explained the effects of partial overlap of the primary junction with the back contact, and have shown how variations in carrier density, carrier lifetime, and CdTe layer thickness impact cell performance.

TABLE OF CONTENTS

FIGURES

TABLES

INTRODUCTION

The objectives of the Colorado State University program have been to (1) quantitatively separate individual performance losses in CdTe and CI(G)S solar cells using existing experimental and analytical techniques, (2) expand the tool set for measuring and separating the losses, and (3) suggest fabrication approaches or modifications to minimize the losses. Much of the work performed during the past 3½ years is described in this report, but in many cases more detailed information can be found on our website www.colostate.edu/orgs/pvlab, in the publications referenced in the final section, and in the specific reports referenced in the final section, most of which are available on request.

The experimental and analytical work described here has largely been done by a dedicated group of graduate students. Jennifer Granata, who worked primarily on impurity studies, and Jason Hiltner, whose work dealt with spatial micro-nonuniformities, have completed their PhDs. Continuing research students include Pamela Johnson, Alex Pudov, Caroline Jenkins, Samuel Demtsu, and Markus Glöckler. Our senior research collaborator Alan Fahrenbruch is now an Affiliate Professor at Colorado State and works closely with the students. Other contributors to the research have included technical support from David Warner and Jay Jablonski, and student projects by Yvonne Shelton, Peter Macedo, and Timothy Nagle.

Prof. Sites' group has actively participated in the NREL-sponsored National CdTe and CIS R&D Teams. It has had productive collaborations with Prof. Sampath's group at Colorado State, as well as with researchers at Aoyama Gakuin University, the Colorado School of Mines, First Solar, Inc., Global Solar Energy, the Florida Solar Energy Center, the Institute of Energy Conversion, International Solar Electric Technology, the National Renewable Energy Laboratory, Siemens Solar Industries, the University of Illinois, the University of South Florida, the University of Toledo, and Washington State University.

WHOLE-CELL LOSS ANALYSIS

Several individual loss-analysis projects for both CI(G)S and CdTe cells have been completed during the subcotract period. The term "whole-cell" is used to indicate that the measurements are averages and not necessarily applicable to all regions of the cell.

CIGS Studies. One example based on the efforts on Alex Pudov is illustrated in the first three figures. Fig. 1 overlays J-V curves from the record-efficiency CdS/CIGS cell [Contreras et al., Prog. in PV **7**, 311 (1999)] with a recent cell made at Aoyama Gakuin University (AGU) in Japan, in which the commonly used CdS window is replaced with wider band gap ZnS to improve the current density [Nakada and Misutani, PVSC **28**, 529 (2000)]. Also shown for comparison is a very high-efficiency crystalline silicon cell from the University of New South Wales (UNSW).

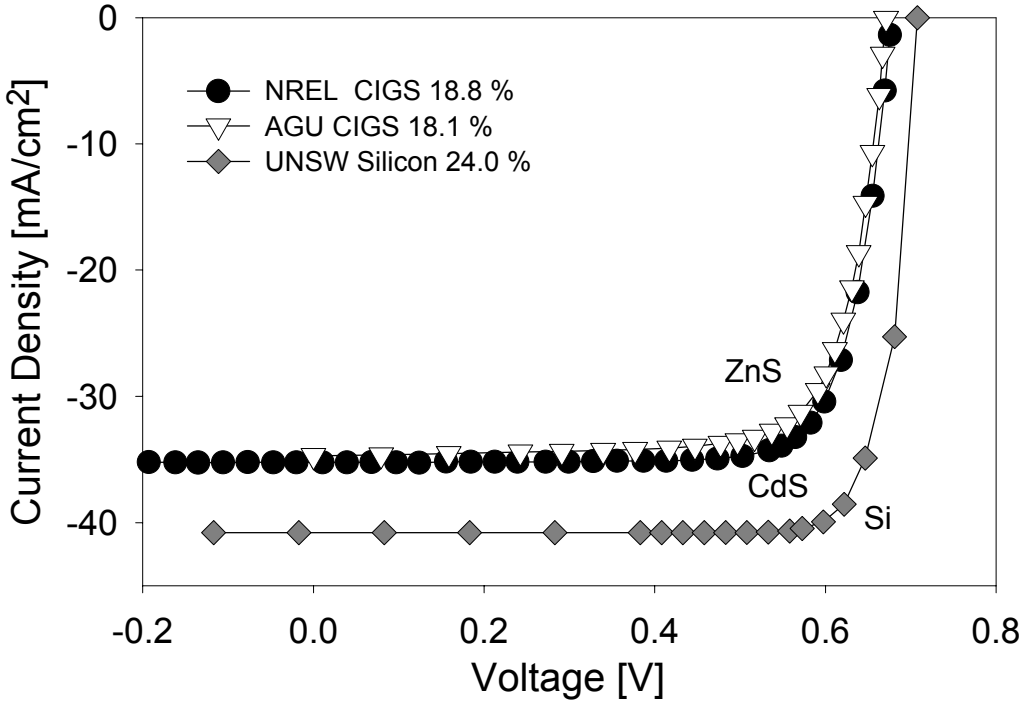

Figure 1. Current-voltage comparison of three high-efficiency cells.

The two CIGS cells are similar to each other, but have smaller current and voltage than the best crystalline silicon cells. More revealing comparisons can be found in the log of

forward current and the quantum-efficiency (QE) curves. The semi-log plot shown in Fig. 2 uses the same data as Fig. 1. The silicon cell has the steepest slope, which corresponds to a diode quality factor A very close to 1.0. The CIGS cells have larger A-factors, about 1.5 for the NREL cell and 1.6 for the AGU cell, which reduces their fill-factors by about 5%. None of the cells is significantly affected by series resistance or shunting.

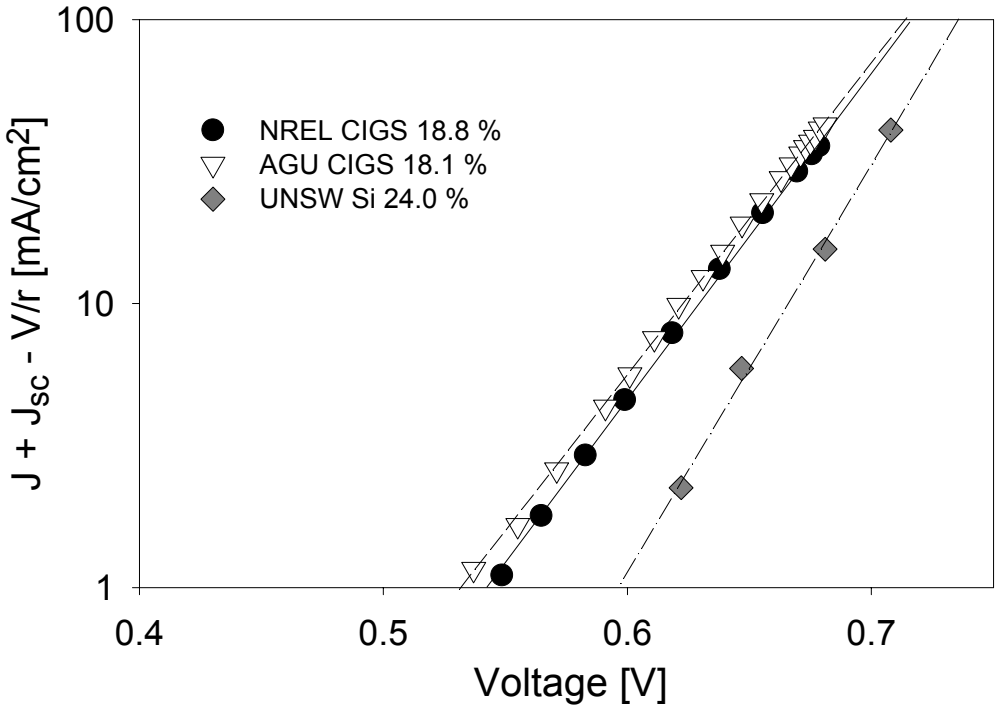

Figure 2. Current-voltage comparison using a semi-log plot.

The QE curves for these cells (Fig. 3) show that the loss in short-wavelength spectral response is in fact about 3 mA/cm^2 smaller for the AGU cell with the ZnS window than for the CdS used by NREL. The crystalline silicon cell has a larger QE at all wavelengths accounting for its larger current density in Fig. 1. The potential improvement from using ZnS with CIGS, however, is counterbalanced by another effect seen clearly in the QE curve. The band gap of the ZnS/CIGS cell is about 1.19 eV, compared to 1.12 for the CdS/CIGS and the silicon cells. Hence, less current is produced by the long-wavelength photons, and the two CIGS cells have nearly the same total photocurrent. The fact (Fig. 1) that the voltages of the two cells are nearly the same

should be interpreted as a superior junction in the lower band-gap NREL cell. A proper comparison of the two CIGS cells would conclude that the ZnS cell has the superior current, because of the larger blue response, but has an inferior voltage in relation to the absorber band gap.

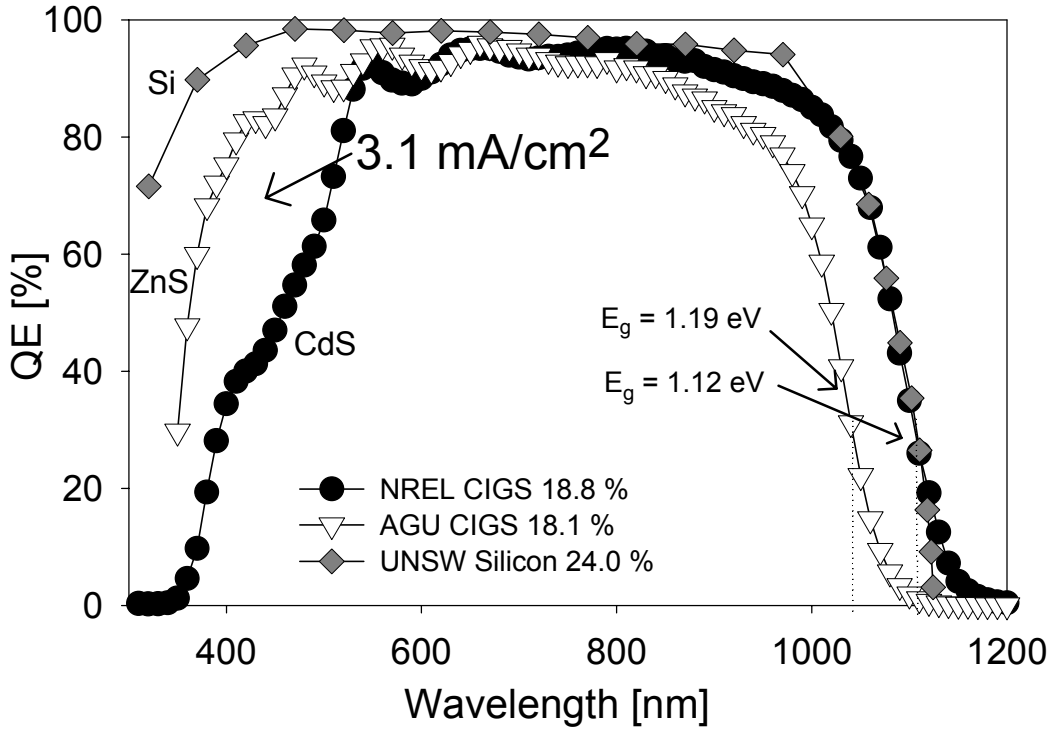

Figure 3. Quantum efficiency for the same three cells.

A second, and somewhat similar, CIGS loss-analysis project was performed by Pamela Johnson in collaboration with Kannan Ramanathan of NREL. In this case, the strategy to replace the CdS window was to omit sulfur from the chemical-growth bath commonly used to grow CdS. The remaining partial electrolyte (PE) was found to introduce sufficient Cd n-doping in the CIGS absorber to form a good homojunction [Ramanathan et al, WCPEC **2**, 477 (1998)]. The J-V and QE curves from such a cell, overlaid with those from an otherwise identical CdS/CIGS cell are shown in Fig. 4. Also shown is the very poor J-V curve obtained when neither CdS nor the partial electrolyte was used. Again with this comparison, there is trade-off in that the CdS cell has a higher voltage,

likely due to less junction recombination, but the non-CdS cell partially offsets this advantage with superior collection of photons with energies above the CdS band gap.

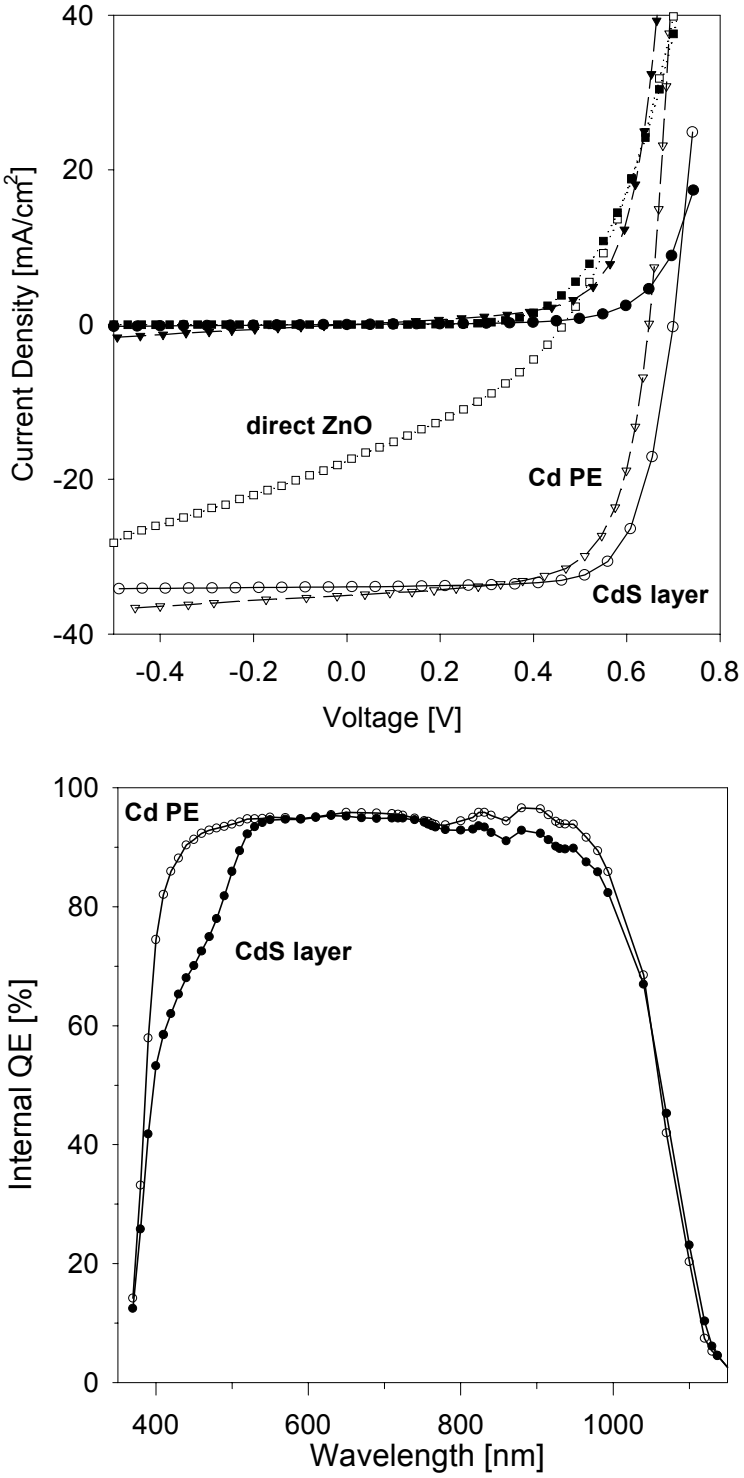

Figure 4. J-V and QE comparison of CIGS cells with and without CdS.

Additional evidence for junction quality can often be attained from capacitance measurements. The inset to Fig. 5 compares the capacitance vs. voltage data (plotted as C^{-2}-V) from two cells made with the partial electrolyte and three with standard CdS. The CdS cells have larger capacitance, implying a smaller depletion width and generally higher carrier density. When absorber carrier density is extracted from the C^{-2}-V slopes and plotted against distance from the junction, a clear distinction is seen. The absorber carrier density is relatively constant for standard-CdS cells, but falls off near the junction when the partial electrolyte is used. The likely physical interpretation is that the partial electrolyte introduces some compensating states, though many fewer than when it is omitted altogether, and these states enhance recombination and decrease voltage. They probably also contribute to the larger shunting seen in Fig. 4.

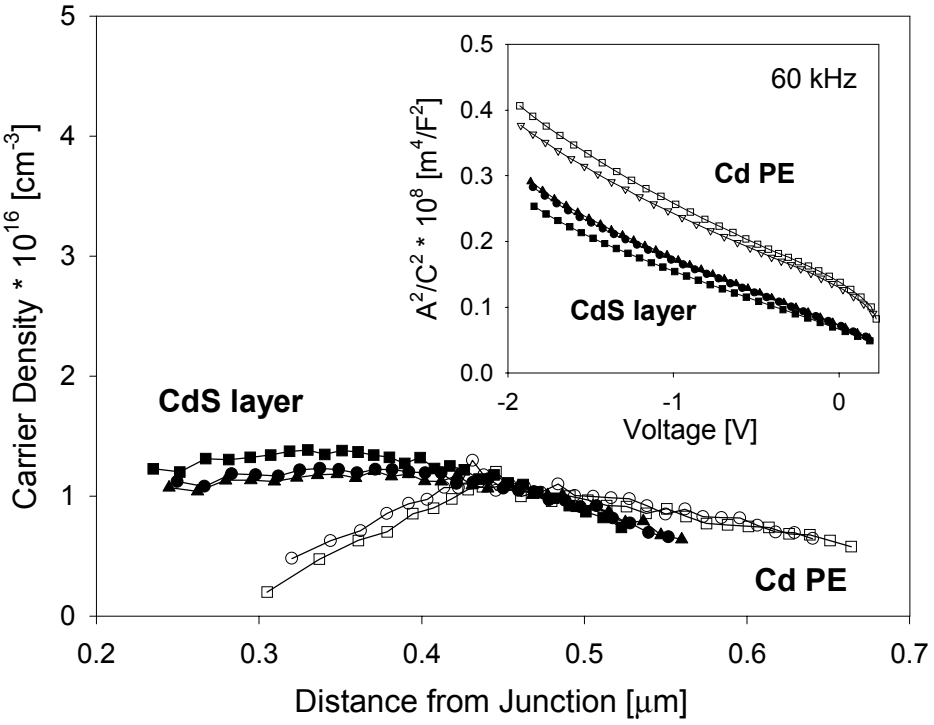

Figure 5. Carrier density profiles for same CIGS cells with and without CdS.

An additional CIGS project done in collaboration with NREL compared cells made with electrodeposition of precursors [Bhattacharya et al, APL **75**, 1431 ((1999)] with physical-vapor-deposition cells. Other CI(G)S loss-analysis projects have involved cells supplied by ISET and Unisun. A related absorber material with wider band gap, $CuIn(Ga)S_2$, has

been under investigation at FSEC, and here also we have participated in the analysis. The CI(G)S projects where we focused on impurity or transient effects will be described in later sections.

CdTe Studies. A local collaboration with Prof. Sampath's group at Colorado State has involved Caroline Jenkins and Samuel Demtsu in loss analysis of these cells. Current-voltage curves are shown in Fig. 6 for a group of five cells on separate 3-in glass substrates taken directly from the air-vacuum-air deposition line. The cells are in the 11-12% efficiency range with voltages near 800 mV and fill-factors near 75%. There is reasonable cell-to-cell consistency among the cells shown, though some of them do show excessive slope near zero bias.

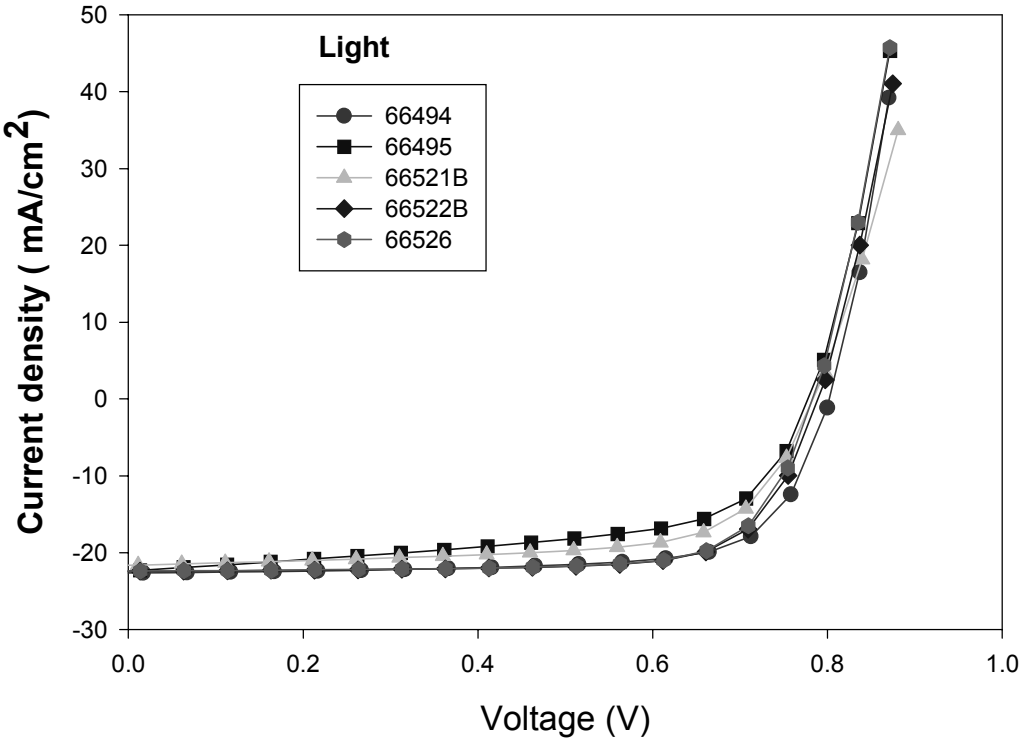

Figure 6. J-V curves from CdTe cells made at Colorado State.

The quantum efficiency curves from this group of cells are similar, and one is depicted in Fig. 7. It shows significant loss in the blue, typical of cells with relatively thick CdS. The band-gap cutoff implies an effective gap energy of about 1.48 eV, somewhat higher

than other CdTe cells and suggestive of only modest sulfur diffusion into the CdTe absorber.

Fig. 7 also shows a subtle feature that we have now found to be common with CdTe cells. Most of the QE curve shows no discernable light-bias dependence, but between 800 and 880 nm, about 40 nm in either direction from the band-gap cutoff, the QE is slightly larger when white-light bias is used. Furthermore, the difference becomes larger as the intensity of the white light is increased. The effect of self-bias from the QE beam, however, should be negligible. The explanation likely involves a modification of the band profile by the white light, but the details will need further work.

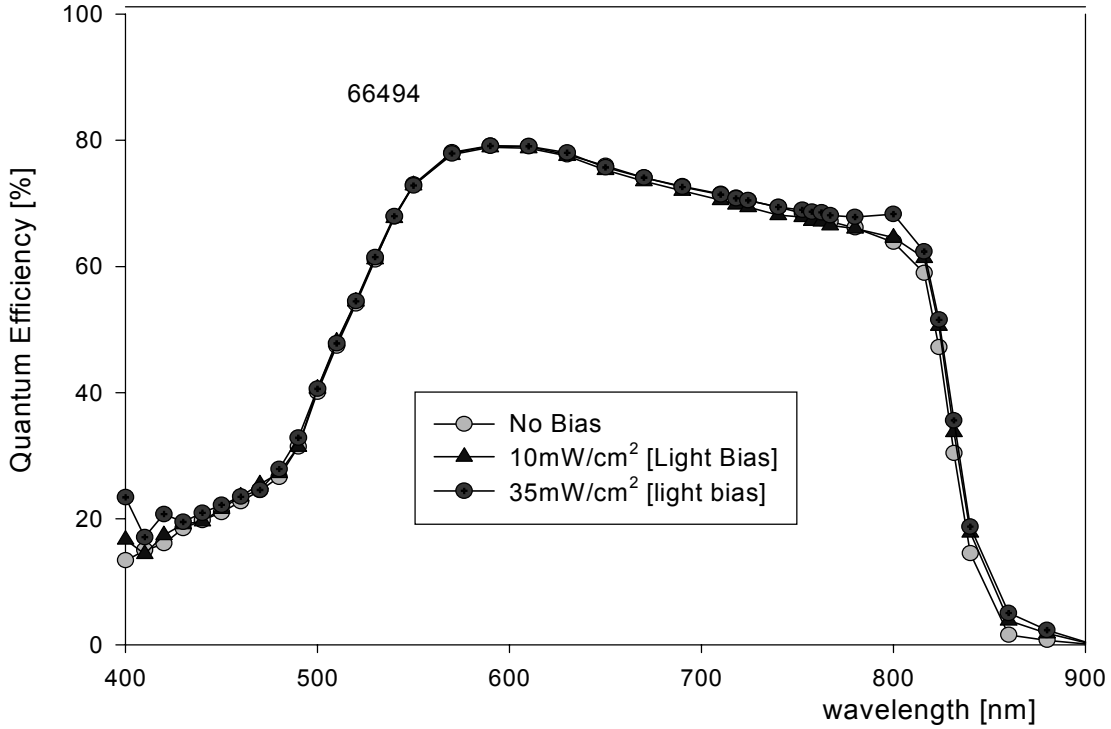

Figure 7. QE curve from one of the Colorado State CdTe cells.

Other CdTe studies have involved collaborations with NREL, First Solar, IEC, and ANTEC. Much of this work involved micro-nonuniformities or changes due to elevated-temperature stress, which will be described in later sections.

IMPURITY EFFECTS

Studies of impurity effects concentrated on the role of sodium in CIS and CIGS cells. A comprehensive description of this work is found in the Ph.D. thesis of Jennifer Granata, and a summary is given here. Sodium was added to CIS and CIGS absorber layers in controlled amounts by coevaporation of $NaSe_2$ with Cu, In, and Se using NREL's physical-vapor-deposition facilities. In each case four Mo-coated substrates were used: (1) soda-lime glass (SLG) (2) soda-lime glass coated with SiO_2, (3) Corning 7059 borosilicate glass, and (4) alumina. The first substrate allowed sodium to reach the CIS because of diffusion through the Mo, the second attempted to block sodium diffusion, and the latter two were nominally sodium free. Inductively-coupled plasma spectroscopy (IPS) and secondary-ion mass spectrometry (SIMS) were used to evaluate the amount and profile of sodium incorporation in the absorber layer. The actual concentrations ranged from about 1 ppm to a few per cent.

In general, there is a distinct improvement with modest amounts of $NaSe_2$, and major deterioration if a large amount is used. In Fig. 8, V_{oc} for the six sodium concentrations on each of the four substrates is plotted against the average sodium concentration of the CIS layer, which includes both that diffused from the substrate and that added in the deposition. There is scatter in the data, but the overall trends are clear. The voltage increases with modest amounts of sodium, has a broad plateau between 0.01 and 0.1 at% but decreases above 1%. The decrease in voltage with large amounts of sodium is accompanied by major decreases in current, especially in the red, and in fill-factor. In this Na-concentration region, the CIS layer has smaller grains and greater porosity.

The variation of a second key parameter, the average CIS hole density derived from capacitance measurements, with sodium concentration is also shown in Fig. 8. In this case, the hole density is near 10^{15} cm^{-3} for sodium concentrations of 0.01 at% and below, increases to the 10^{16} range for 0.1 – 1 at%, after V_{oc} is saturated, and becomes very large for higher concentrations where the morphology changes are observed.

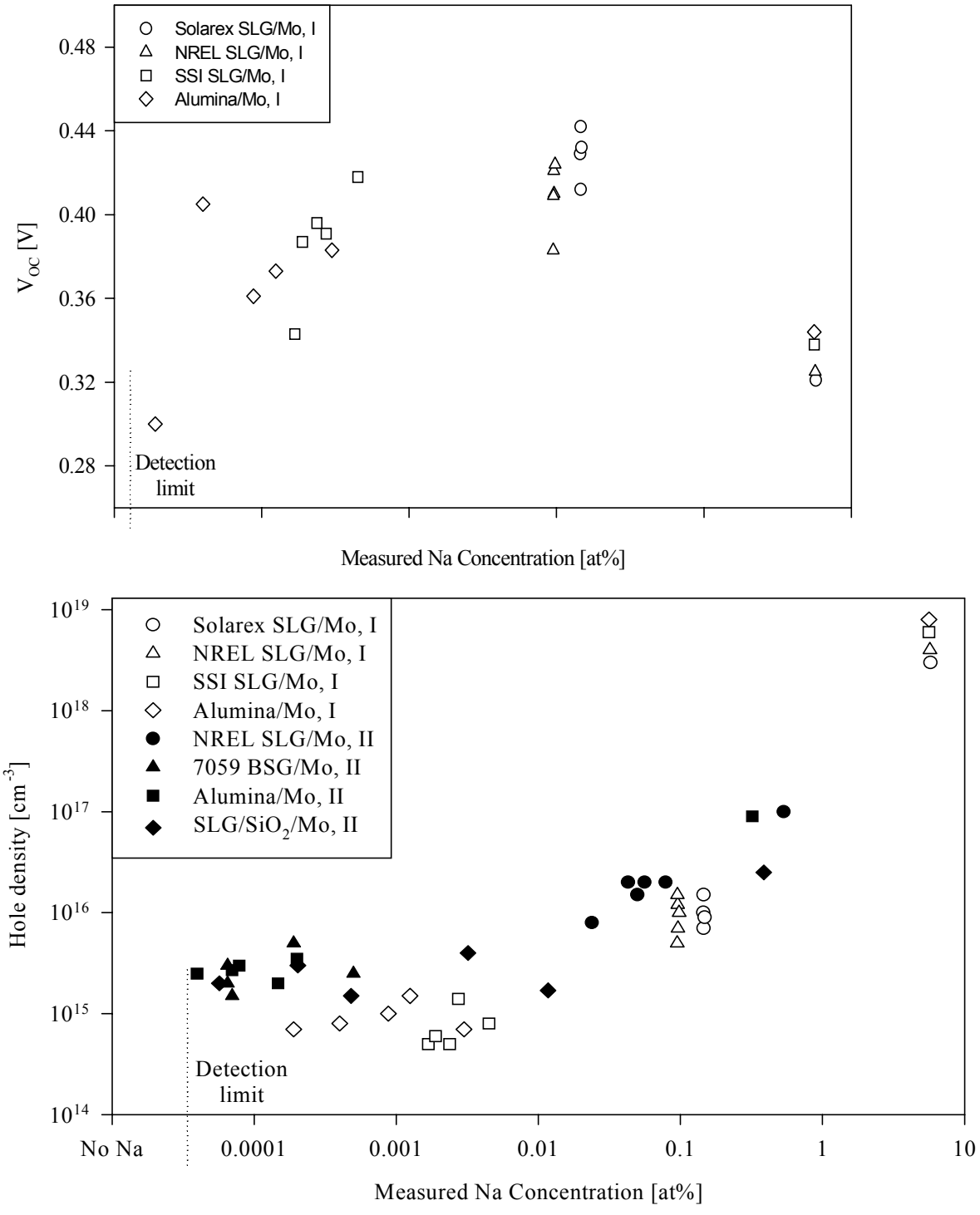

Figure 8. Variation in CIS open-circuit voltage and hole density with sodium concentration for four substrate materials.

Improvements in CI(G)S cell performance with sodium addition have been seen by several groups, but there has not been agreement on the mechanism responsible. We believe it is a grain boundary effect, because (1) there is direct Auger evidence of Na at the boundaries, but not in the bulk crystallite, (2) SIMS shows more total Na present with small-grained material than large, (3) increased V_{oc} implies less forward-current recombination, which is assumed to be primarily determined by grain boundary states, and (4) increased hole density usually implies reduced compensation, also associated with grain boundary states.

Assuming, however, that the sodium responsible for better performance resides at the grain boundaries, there are at least three possible mechanisms: (1) It may directly help passivate the granular surface by reducing the number of uncoordinated In bonds. (2) It may indirectly passivate the surface by acting as a catalyst for oxygen, which would passivate the uncoordinated In bonds. (3) It could act as a surfactant during growth to inhibit formation of structures with compensating states or would yield generally larger crystallites. Future work should include systematic oxygen background control, variations in the sodium effect with gallium concentration, and similar investigations of impurities other than sodium.

SPATIAL MICRO-NONUNIFORMITIES

Apparatus. The use of polycrystalline materials necessitates uniformity considerations not generally at issue with single-crystal solar cells. Investigation of the spatial uniformity of photocurrent collection has been aided significantly by an apparatus developed by Jason Hiltner [see Publications 9, 11, and 13], which features 1 μm spatial resolution with near-solar incident intensities. Observations provided by the instrument include the overall uniformity of collection, as well as more detailed characterization of the cause of local reductions in response. The apparatus is shown schematically in Fig. 9.

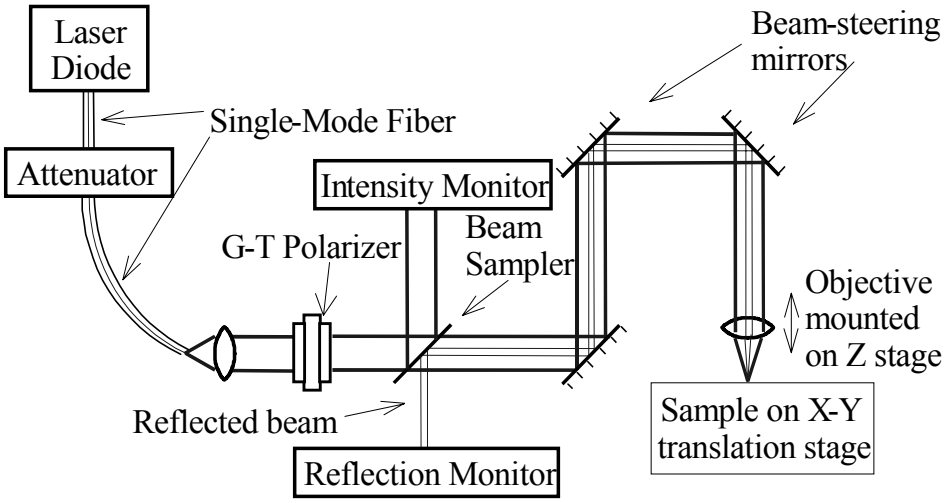

Figure 9. Schematic of spatial-nonuniformity apparatus

Multiple lasers in the 635-830 nm range can be easily selected by changing the fiber-optic connectors. The spot profile and location are unchanged when different lasers are selected. In addition, one laser temperature-tuned through the 825-857 nm range allows measurement of local variations in the quantum efficiency near the CdTe band gap. Electronically modulated laser output is coupled into a single mode fiber, then passes through an electronic attenuator variable over four decades, a beam expander, a polarizer, and a beam splitter to monitor direct and reflected beams. The beam is then steered by

mirrors onto a high-quality microscope objective lens that features an adjustable correction collar for use with superstrate cells and produces a beam neck just under 1 μm.

The cell positioning equipment consists of three high-resolution translation stages. A board-level control corrects for backlash and allows repeatability of 1 μm even after a cell has been removed and remounted. Photocurrent from the cell is converted to voltage and measured with a lock-in amplifier. LabView™ software is used to control the positioners, attenuation, and cell bias. A single screen displays the collected data in real time. Data is typically collected over a large (5-mm square with 100-μm laser spot), intermediate (500-μm square, 10-μm spot), or small (50-μm square, 1-μm spot) area.

Examples of small-area photocurrent maps are shown in Fig. 10 with intensity close to one sun and numerical scales approximately the local quantum efficiency. Shown are a single--crystal GaAs cell with no discernable variations, a typical good-quality NREL CdTe cell, and an NREL CdTe cell fabricated without the usual $CdCl_2$ annealing step.

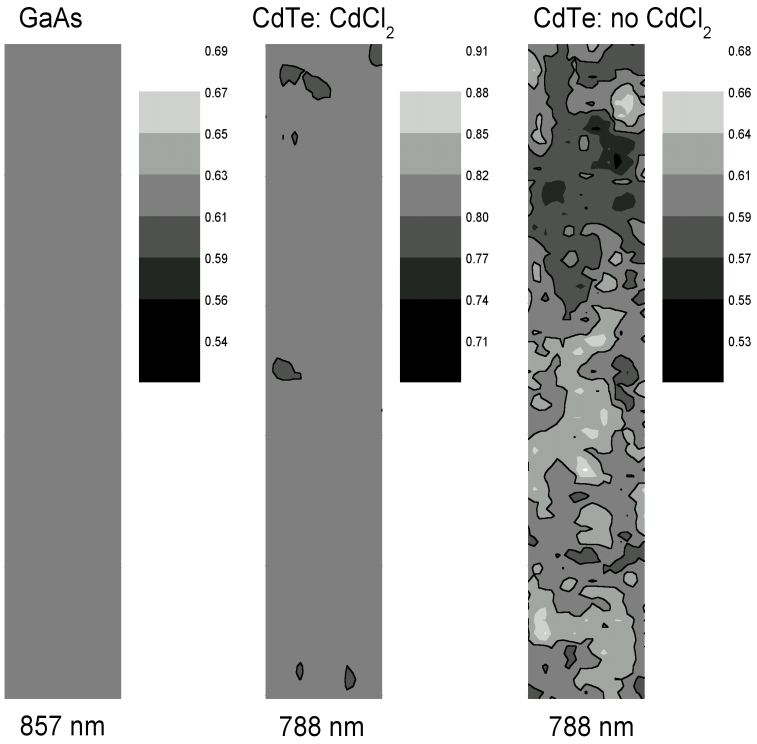

Figure 10. Photocurrent over 10 by 50 μm area for three solar cells.

Reproducibility of features is quite good and is illustrated in Fig. 11. The top graph shows the photocurrent response of a 1 μm beam stepped across a well-defined slit, and the bottom graph shows the effect of a less well-defined gridline. Note that in this case the response is very nearly identical when the spot is stepped back in the opposite direction.

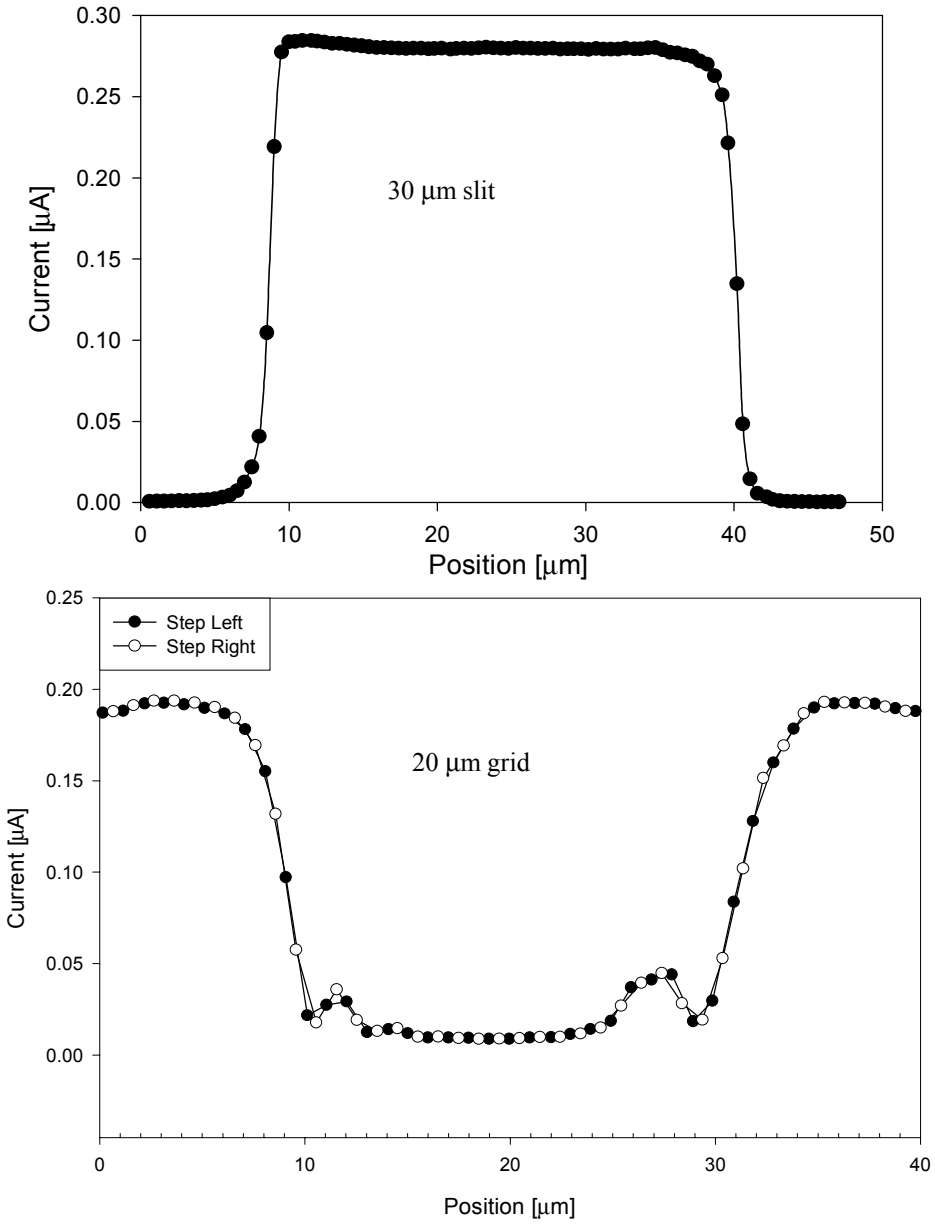

Figure 11. CIS response to spot stepped across a slit (top) and a grid line (bottom).

Another possible concern about reproducibility is the possibility that the light spot might change in size, or possibly shift in position, when one switches to a different wavelength laser. However, Fig. 12, which gives the photocurrent response of a cell below a 5 μm pinhole for two of the lasers available, shows that neither the falloff in intensity at the pinhole edges nor the position of the pinhole is significantly changed when a different laser is used.

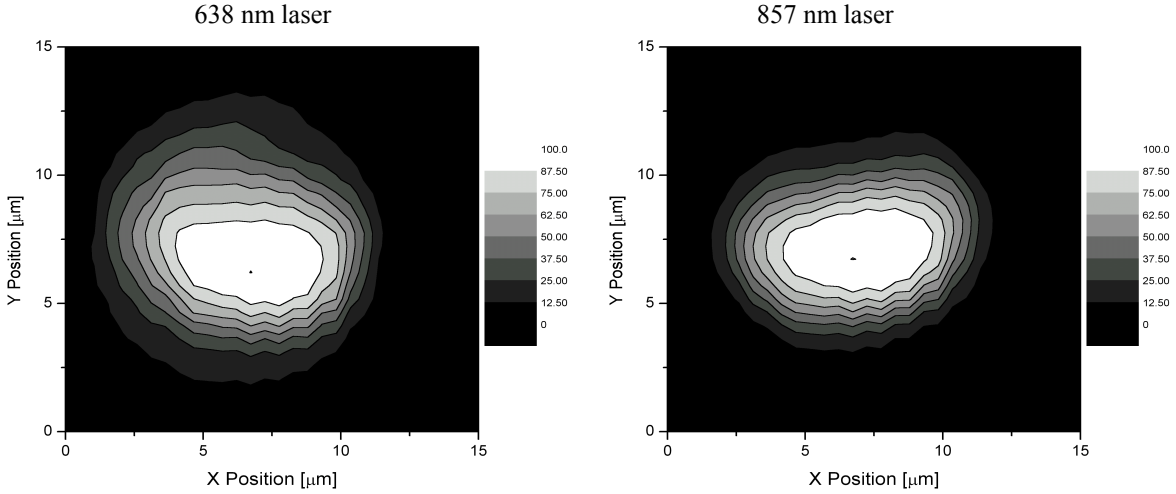

Figure 12. Normalized power through a 5-μm pinhole for two lasers.

CdTe Studies. Local variations in the photocurrent from a good-quality NREL CdTe cell, such as the middle representation in Fig. 10, are fairly modest for photon energies above the CdTe band gap. The 788-nm wavelength used in Fig. 10 corresponds to an energy of 1.57 eV, which is well above the CdTe gap. As the photon energy is reduced, however, the spatial variations in photocurrent become much larger, as illustrated in Fig. 13. The area shown is again 10 by 50 μm, and the same area is shown for each wavelength. The spot size is 1 μm, and its intensity is comparable to one sun. The variable temperature laser is used to achieve the seven wavelengths between 825 and 857 nm which span the CdTe band gap. As the photon energy is decreased (increasing wavelength), the variations become much more pronounced, and they reach a factor of four in the right-most mapping.

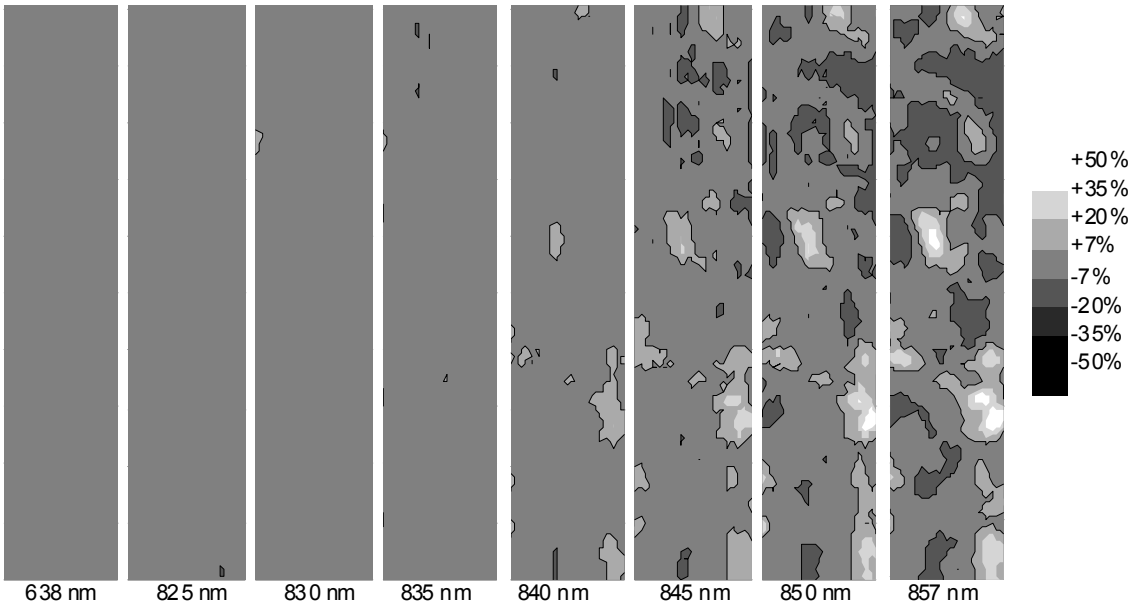

Figure 13. Photocurrent response over a 10 by 50 μm area at several wavelengths.

The explanation for the dramatic change seen in Fig. 13 [Hiltner and Sites, MRS Proc. **668**, H9.8 (2001)] is that there are regions where significant amounts of sulfur have diffused into the CdTe, and the lower band-gap $CdTe_{1-x}S_x$ allows collection from longer wavelength photons. Most likely the physical regions of large sulfur diffusion correspond to the grain boundaries. The CdTe cell in Fig. 10 that was not treated with $CdCl_2$ does not show large changes in the photocurrent mapping, and hence band gap, which strongly suggests that the variations in band gap are a result of the CdTe treatment. Thus the $CdCl_2$ both improves the electrical quality of the junction and enhances the interdiffusion at the grain boundaries.

The response of a single area on the same $CdCl_2$-treated NREL cell shown in Fig. 13 was also mapped before and after 10 days of elevated-temperature (100°C) stress. The cell as a whole exhibited losses in open-circuit voltage, fill-factor, and short-circuit current as will be described in the following section. Fig. 14, however, shows the photocurrent map taken over a 500- by 500-μm region taken with a 10-μm spot size. The region was deliberately chosen to have a prominent initial defect that could be used for reference. This low-photocurrent defect is clearly seen in the upper-left pre-stress map taken with a

photon energy far above the CdTe band gap. After stress, and using the same photon energy, much of the area is unchanged, but several additional low-photocurrent regions appear, indicating a non-uniform degradation of the cell. At a photon energy just below the CdTe band gap, however (lower map), the degraded areas show a higher photocurrent, which again indicates the presence of significant sulfur mixing and the lower band-gap $CdTe_{1-x}S_x$ alloy.

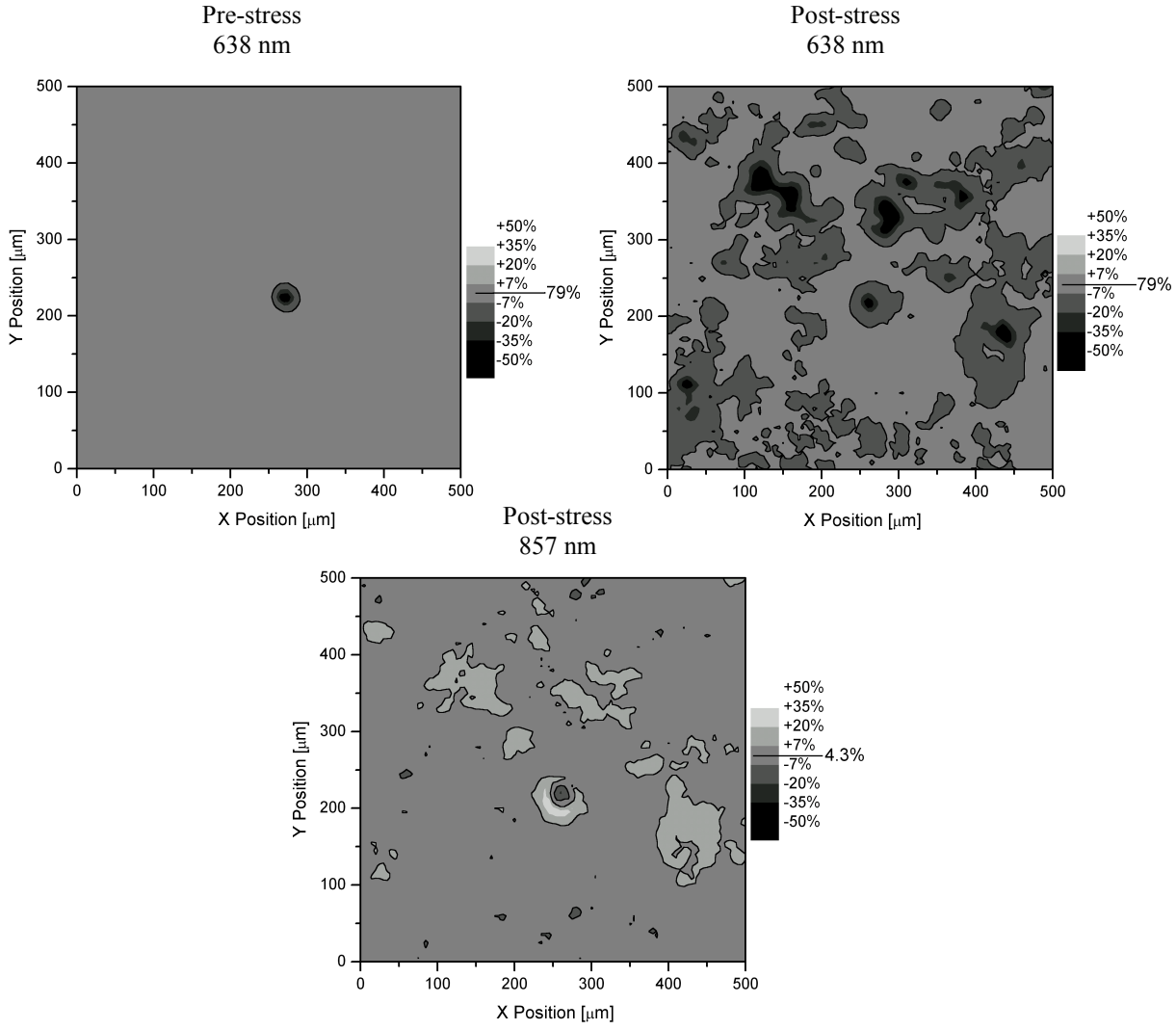

Figure 14. CdTe photocurrent maps before stress and at two wavelengths after stress.

The proposed interpretation of Fig. 14 is that there are regions of the cell, presumably associated with grain boundaries where species can diffuse more rapidly. Hence, the increase in band gap associated with sulfur diffusion takes place at the same locations as degradation resulting from a different process, likely related to the movement of copper as discussed in the following section.

ELEVATED-TEMPERATURE EFFECTS

Both CdTe and CIG(S) cells have been held at various bias and illumination conditions while exposed to elevated temperatures for time periods ranging from hours to months. An example of the local changes in CdTe cells was given just above in the previous section. Here we will discuss several whole-cell results.

CdTe Elevated-Temperature Stress. Changes in CdTe-cell performance, known to occur in many cases at temperatures of 100°C and above, has been a manufacturing concern. Significant effort, especially by Jason Hiltner, has been devoted to understanding what factors are responsible and how the changes can be minimized. A typical evolution of J-V curves is shown in Fig. 15 for a CdTe cell that was held under illumination for various times at open-circuit voltage and a temperature of 100°C.

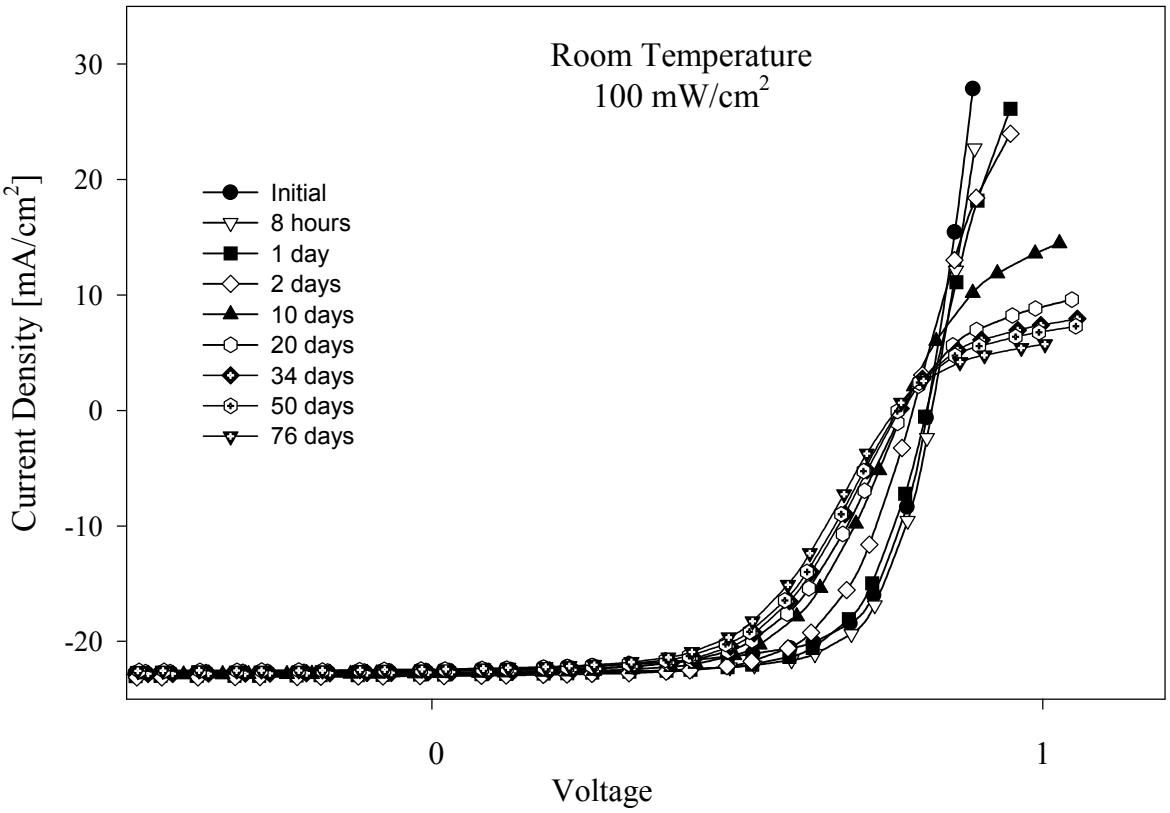

Figure 15. Temperature-induced J-V changes in an NREL CdTe cell.

The primary performance parameter that changes in Fig. 15 is the fill-factor, but it is clear that the curves are also becoming significantly current-limited at forward currents. This latter effect is often referred to as "rollover" and is characteristic of a second diode barrier with polarization opposite the primary diode barrier [Stollwerck and Sites, EPSEC **13**, 2020 (1995)]. Close inspection shows that the voltage in Fig. 15 is also somewhat reduced. For cells more susceptible to stress, the voltage decrease becomes more significant, and the current also starts to decrease.

Fig. 16 [Hiltner and Sites, AIP Conf. Proc. **462**, 170 (1998)] shows that for small stress times the cell efficiency increases slightly, perhaps due to an improvement in cell quality with annealing. At some point, however, the efficiency begins a steady decrease. Both the initial increase and the later decrease are due almost entirely to changes in fill-factor. The cells shown in Fig. 16 were made by Solar Cells Inc., now First Solar Inc., but qualitatively similar results are found with NREL CdTe cells.

At a constant bias, the time scale of the efficiency changes is a strong function of temperature. At lower temperatures, the onset of the decrease occurs at a later time and the rate of the decrease is less, as seen in the top part of Fig. 16 for open-circuit voltage. The changes in efficiency, however, are also a strong function of bias, as seen in the lower two sections of Fig. 16. In the middle section, the four cells are held at 100°C in the light, but one is at maximum power (MP), one at short circuit (SC), one in reverse bias ($V < 0$), and one at open circuit (OC). The MP and SC conditions show the smallest change in efficiency, while OC shows the greatest change. The bottom section shows a similar effect when cells are kept in the dark at 100°C. In this case, the cell held at $V = 0$ changes little, while that farthest in forward bias ($J > 0$) changes the most.

Fig. 17 summarizes the efficiency changes seen in a group of nominally identical NREL cells. Here the pattern is clear. Cells at zero or modest forward bias, light or dark, change the least, while those at higher forward bias or in reverse bias change the most. Fig. 17 also shows the effect of different back contacts, which will be discussed below.

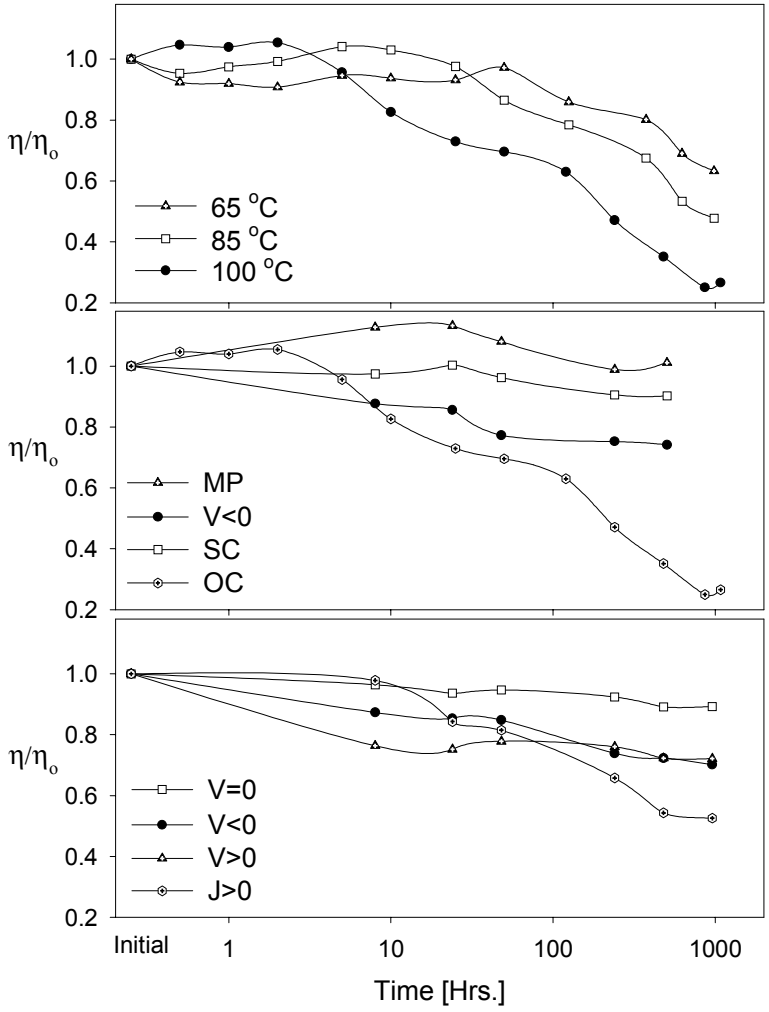

Figure 16. CdTe efficiency vs. stress time. Top: three temperatures (light), Middle: four biases (light), Bottom: four biases (dark).

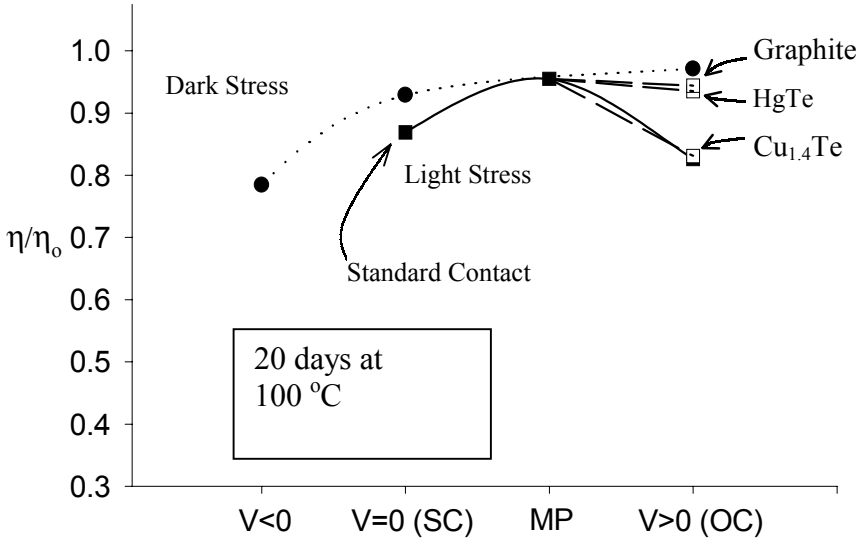

Figure 17. Bias dependence of efficiency changes.

Data on cells from both SCI and NREL have been evaluated with an activation-energy model to yield an acceleration factor, the ratio of time for changes at normal operating temperature to that at stress temperature T_s. The acceleration factor is shown in Fig. 18, as well as a typical profile of field temperatures used to establish the effective operating temperature T_{eff}.

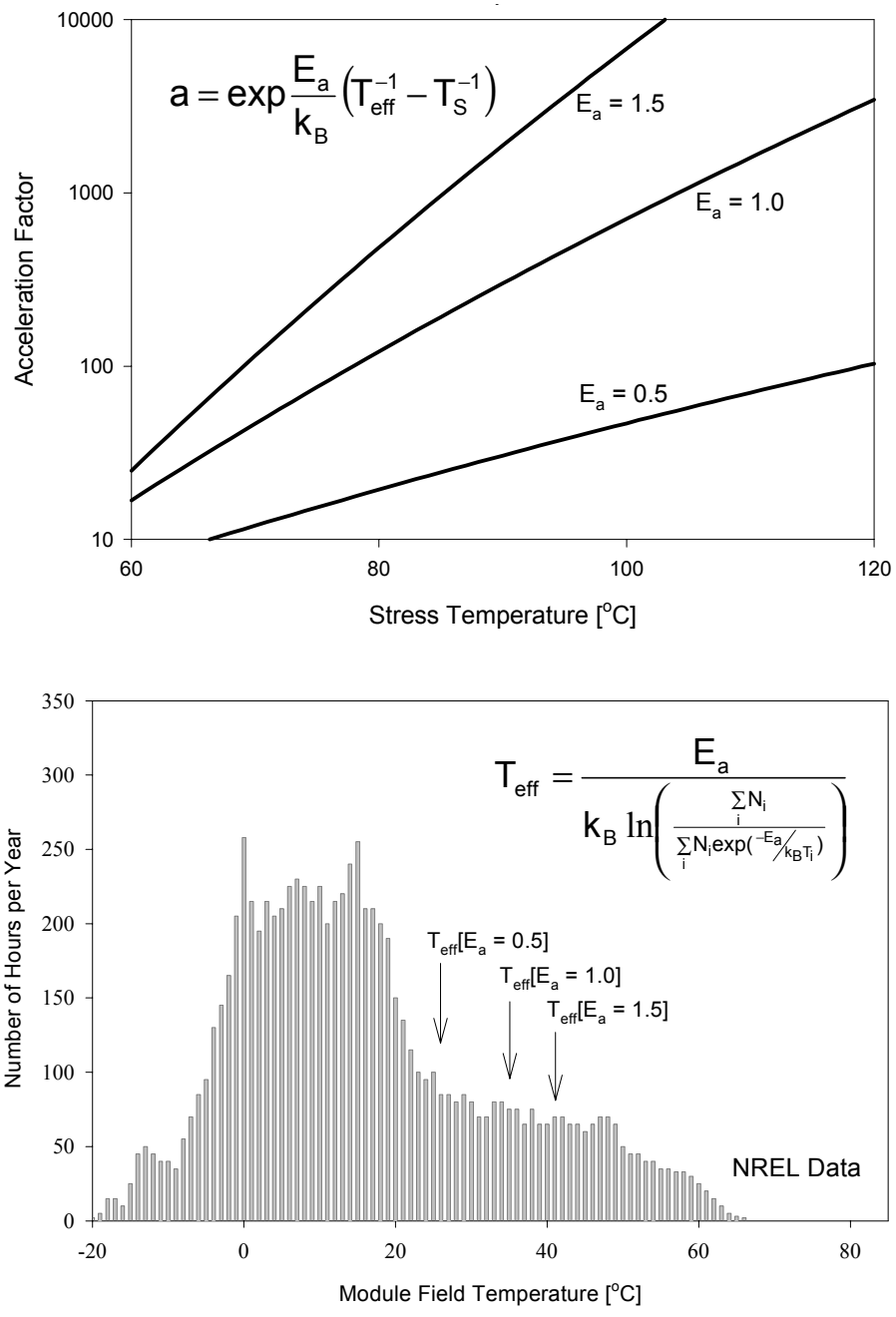

Figure 18. Acceleration factor from activation-energy model.

The activation energy established from data such as shown in the top section of Fig. 16 is typically near 1 eV. Hence the acceleration factor for 100°C stress and the operating profile show in Fig. 18 is roughly 500. Thus, under normal operating conditions, the changes shown in Fig. 15 should take place over 100 years rather than the 76 days at the elevated temperature.

The changes in CdTe J-V curves are clearly related to the copper used in the back contact [Asher et al., PVSC **28**, 479 (2000)]. A major contribution to this conclusion from the work of our group is shown in Fig. 19. In this case, four otherwise identical CdTe cells were made at NREL with different amounts of copper used in the back contact. These are expressed as the ratio of the copper-containing material to the graphite paste it was mixed with. All the cells used in Fig. 19 were stressed under illumination at 100°C and open-circuit voltage.

Starting from the upper left in Fig. 19, the smallest amount of copper leads to the smallest change in J-V in the power quandrant. On the other hand, this cell develops the largest amount of "rollover" during the elevated-temperature stress. Conversely, the cell with the most copper (lower right) shows the greatest performance change, but the smallest amount of induced "rollover". The two cells with intermediate amounts of copper complete the pattern.

The highly probable explanation for the two effects seen in Fig. 19 is that copper diffuses out of the back contact towards the primary junction and is responsible for two effects. One is the depletion of copper in the back contact, which increases the contact barrier and thus enhances the "rollover", as will be discussed in the following section on cell modeling. It also reduces the fill-factor somewhat. The second, and generally more serious, effect is the degradation on the primary junction, which is seen in the reduction in open-circuit voltage of the two cells with the larger amounts of back-contact copper. The rate at which the copper diffuses is governed both by temperature and by internal field, which varies with bias.

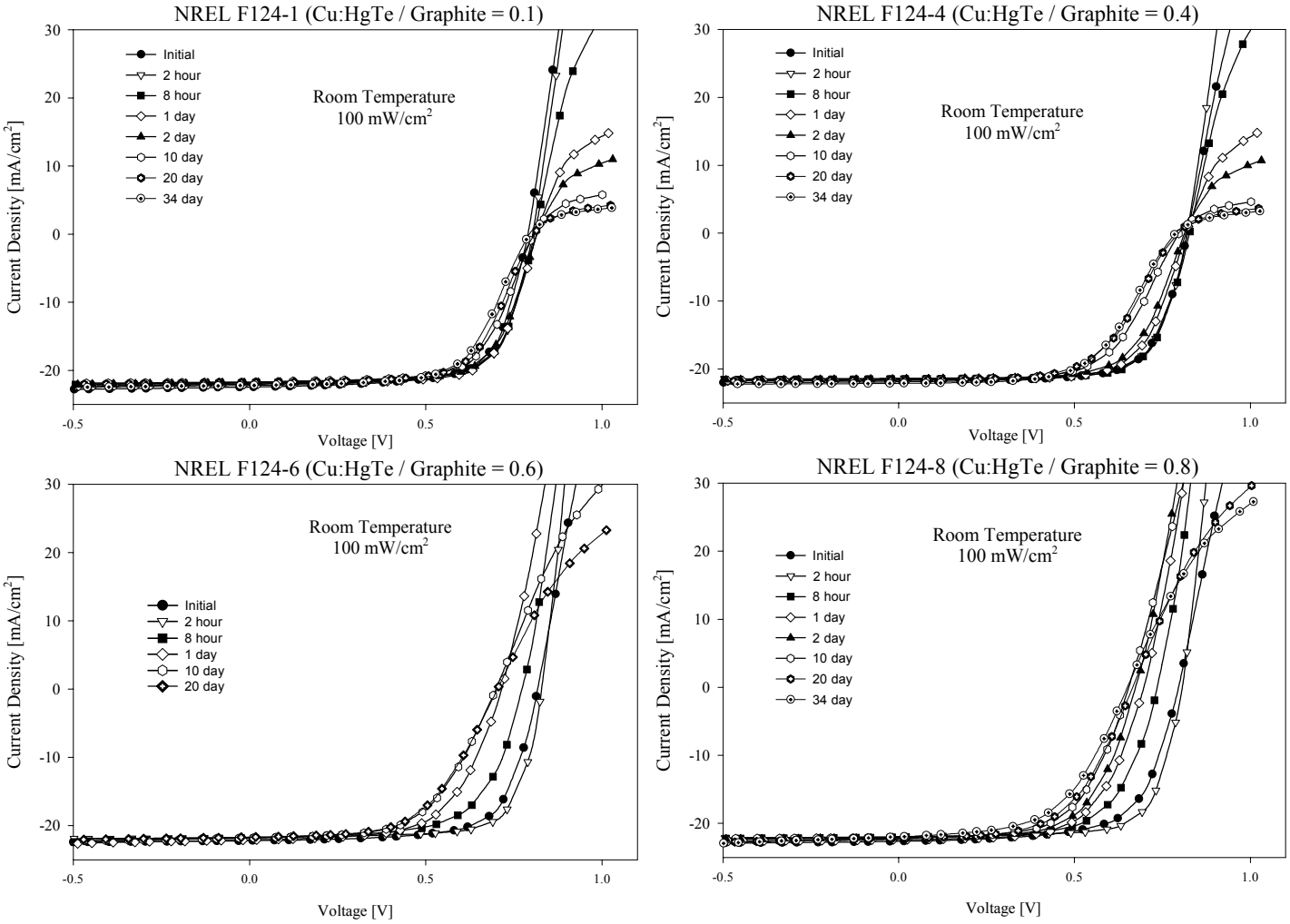

Figure 19. J-V changes in CdTe cells with varying back-contact copper.

CI(G)S Transients. Near-reversible transient behavior is seen in many CIS and CIGS cells. Cell performance generally improves under illumination and falls off under dark heat. In many cases, the effect is small, but for cells made with Siemens Solar Industries (SSI) absorbers, it can be significant. A series of transient experiments have been performed by Pamela Johnson in collaboration with Dale Tarrant of SSI.

A typical transient cycle consists of holding a cell under illumination, hence open-circuit voltage, for 20 hours at ambient temperature, then 20 hours in the dark with V = 0 at 80 to 100°C. The typical changes in the J-V curve and the hole-density profile deduced from capacitance measurements are shown in Fig. 20. The top part of the figure shows that the initial current-voltage curve of a standard SSI cell softens considerably during the dark heating, but recovers during the light exposure. Subsequent temperature cycles show an approximate repetition of the two curves. The major performance change is in the fill-factor, and it is accompanied by a "rollover" appearance in the first quandrant. The voltage can also decrease slightly, but the current is essentially unchanged.

The lower part of Fig. 20 shows the effect of absorber hole density during similar cycling. In this case, the cell consists of an SSI absorber covered with high-resistivity ZnO and no CdS. The spatial dependence of the absorber hole density is deduced from capacitance-voltage measurements. Here also there is a clear difference between the curve following light exposure (again at open-circuit voltage) and that following the dark soak at V = 0. The hole density following the light exposure is about three times larger, and again the second cycle nearly repeats the first-cycle data. The correlation of the larger carrier density with the better performance is consistent in our experience with thin-film polycrystalline cells.

Fig. 21 extends the temperature cycling over several cycles and shows the effect on fill-factor. When it appeared that the 20-hr light soak was not sufficient to return the cell fully to its initial condition, the light soak was extended, and after 200 hours, the fill-factor had indeed returned to its initial value.

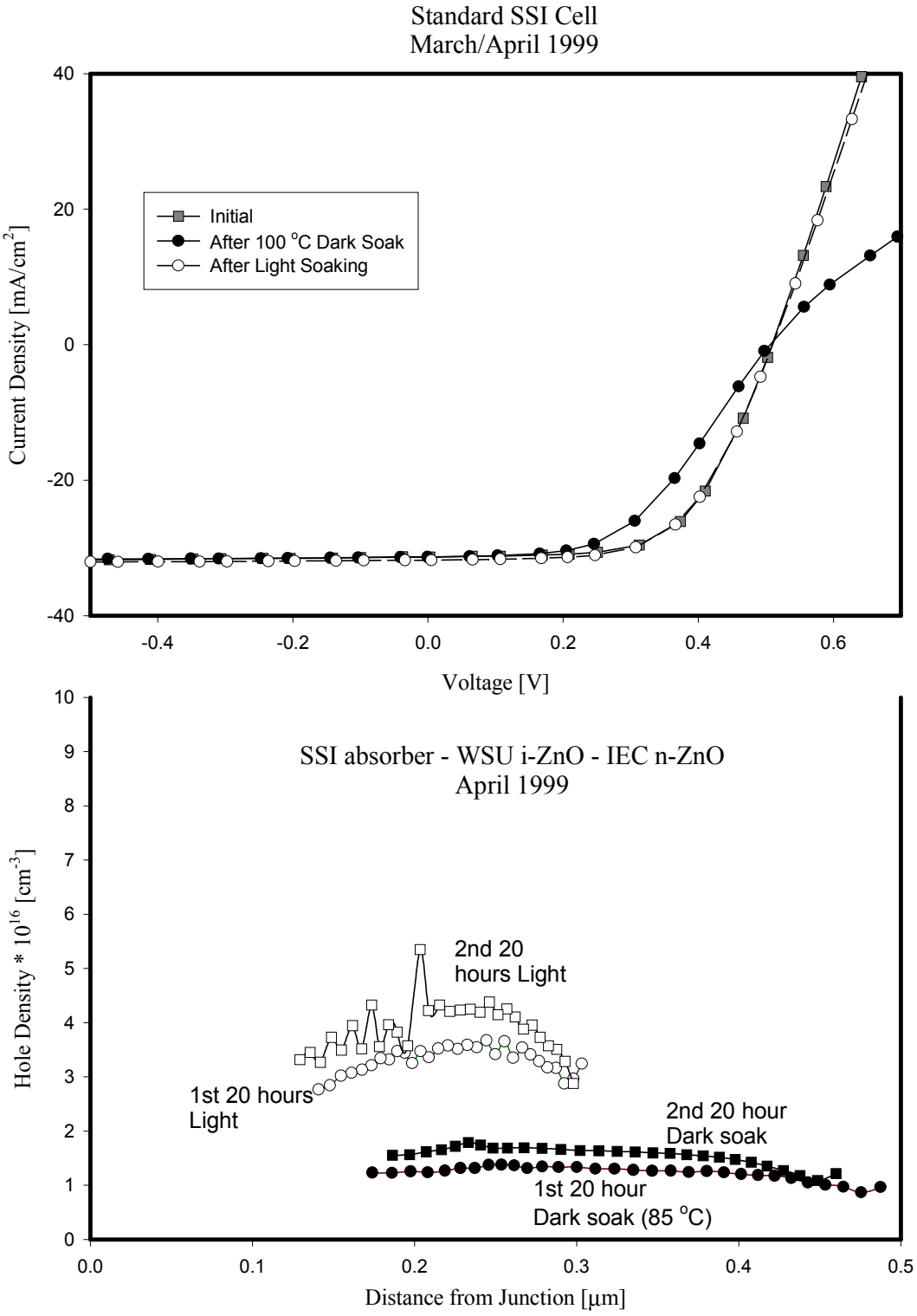

Figure 20. Transient behavior of SSI-absorber cells following elevated-temperature dark and light soaking. Current-voltage at top, hole density at bottom.

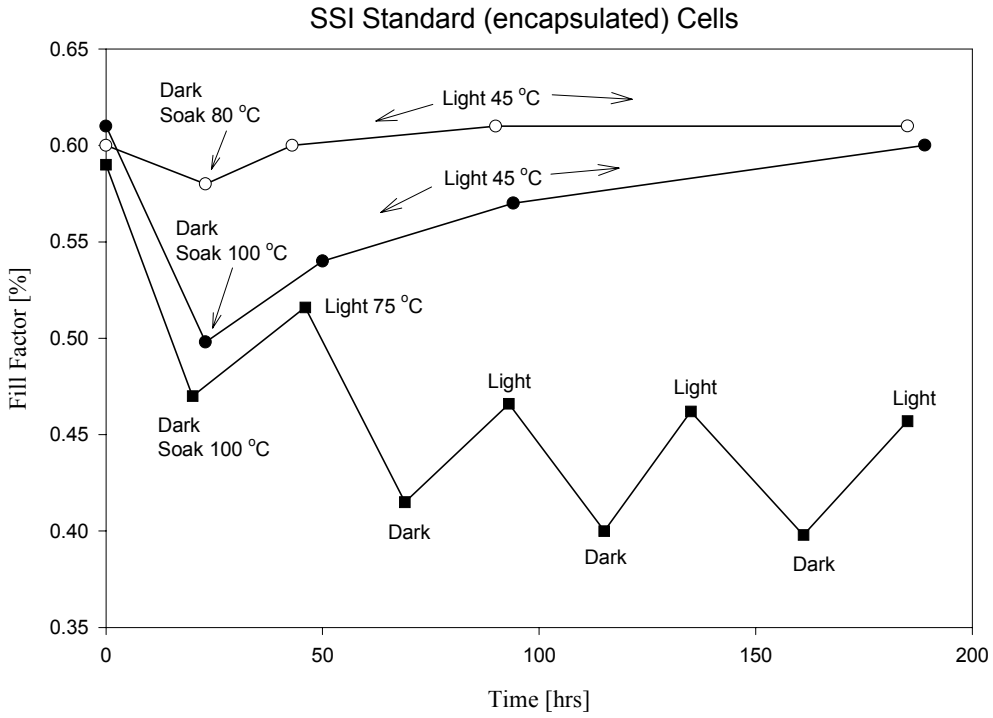

Figure 21. Fill-factor transients in SSI cells.

Since the cycle defined above involved both a change in illumination and a change in cell bias, it was not obvious which was driving the changes seen in Figs. 20 and 21. To separate the two possibilities, nominally identical cells on a common substrate were subjected to voltage cycles. One cell was held in the dark the whole time, and its voltage was cycled between open-circuit and zero. The other cell was cycled between light and dark, which induced the same voltages. The results are shown in Fig. 22, where dark exposures are shown with a solid line and light exposures with a dotted line.

As expected, the open-circuit voltage of both cells in Fig. 22 changed very little following any of the cycles. The fill-factor, however, again showed the typical cyclic behavior, but the pattern was much the same whether or not the open-circuit part of the cycle was under illumination. Changes in capacitance curves with voltage were also little affected by the presence of the light. Thus, it seems clear that the transients seen in the SSI-absorber cells are driven by voltage rather than by illumination.

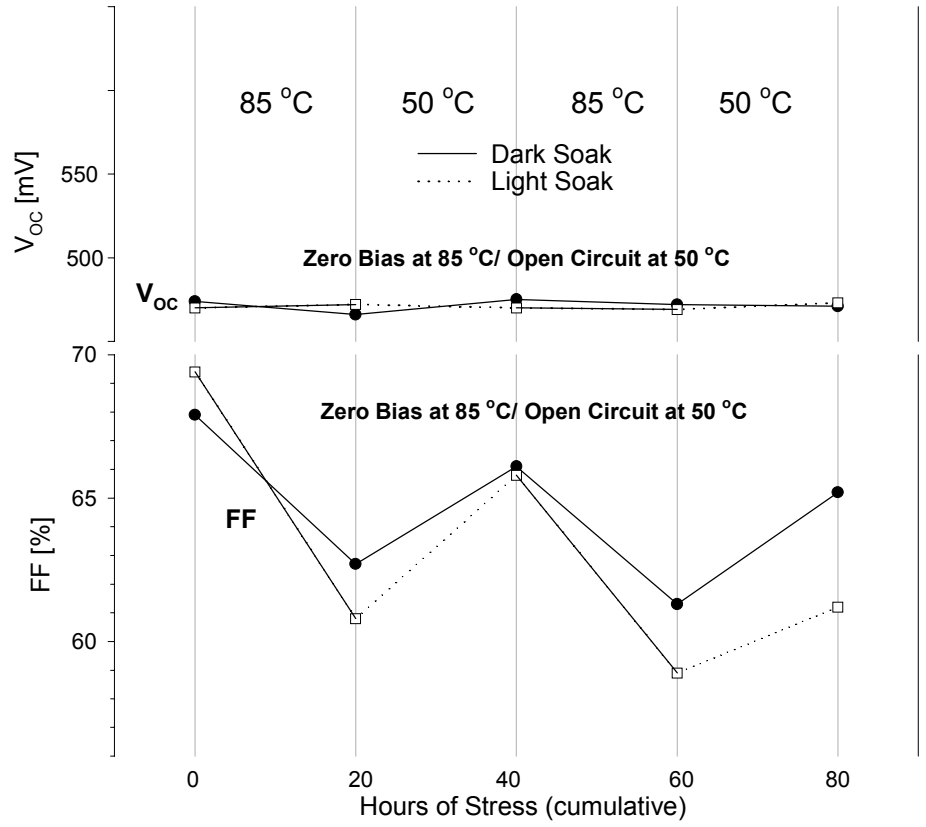

Figure 22. Voltage and fill-factor response to cyclic bias.

A recent extension of the transient work has been to combine it with capacitance-frequency measurements made at different temperatures to gain information on trapping-state energies, densities, and spatial locations. Again a major change is seen in cells with SSI absorbers between the data following a light (forward bias) and a dark (zero bias) soak. One set of such curves is depicted in Fig. 23. The average trap response frequency can be deduced from the steepest part of the transition between low and high frequencies, and the trap density can be taken from the change in capacitance. As can be seen qualitatively from Fig. 23, the cycling causes a major difference in response frequency, but there is relatively little change in the trap density itself with either the cycling or with temperature. Additional analysis [Johnson et al., MRS Proc. **668**, H5.12 (2001)] can be used to extract the energy of the traps involved. The result is that the traps following the dark soak appear to be deeper in the band, which would be consistent with a lower carrier density.

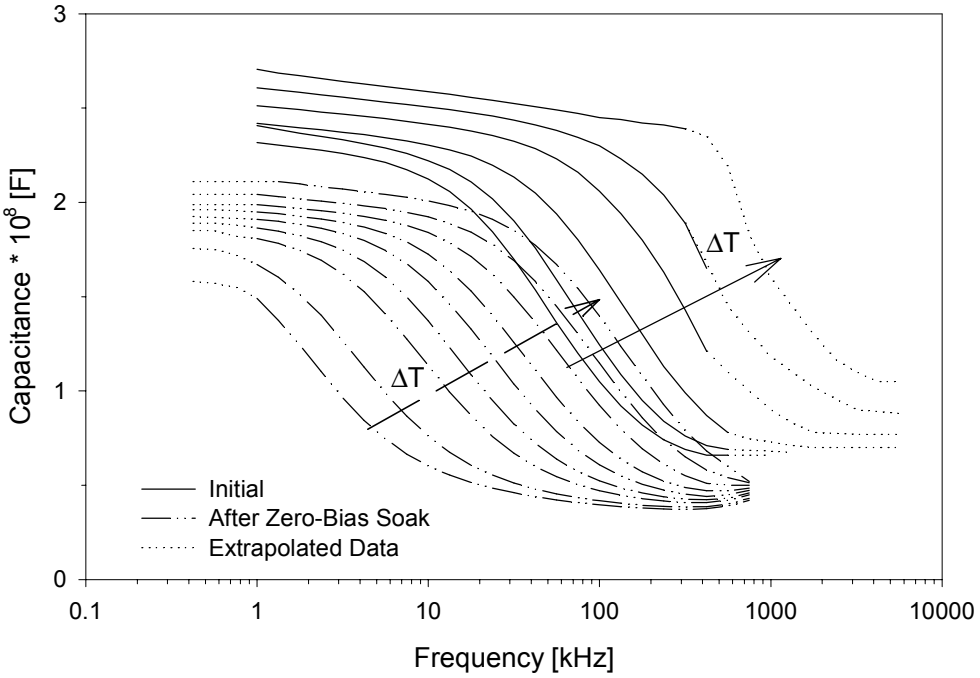

Figure 23. Transients in capacitance vs. frequency curves taken over a temperature range from 220 to 295 K.

COMPUTATIONAL MODELING

The purpose of computational modeling is to visualize the band structure, carrier transport and recombination, and ultimately the current-voltage curves of simulated solar cells based on realistic parameters taken, or at least suggested, by experimental data. The calculations presented in this section were done by Alan Fahrenbruch and were focused on the CdS/CdTe cell structure. The software used was AMPS-1D (version 1,0,0,1) written under the direction of S. Fonash at Pennsylvania State University with funding from the Electric Power Research Institute. One significant enhancement in version 1,0,0,1 is that the number of wavelengths used has been increased, which allows more detailed analysis near the band-gap cutoff.

Input Parameters. The absorption coefficients for CdS and CdTe were taken from Rothwarf and Boer [Prog. Sol. State Chem. **10**, 71 (1975)]. There is generally very little difference seen between the single-crystal and the polycrystalline absorption spectra. The illumination spectrum assumed was ASTME 892 AM1.5 Global normalized to 100 mW/cm^2. The calculations assumed the minimum number of material layers considered necessary to reasonably replicate a CdTe cell: front contact, n-CdS, p-CdS_xTe_{-x}, p-Te, and back contact. It was found that the assumption of a single CdTe layer yielded results very similar to earlier calculations with three sub-layers of CdTe. A summary of the parameters used for the individual layers are given in Table 1. The ones that were varied during the studies reported are indicated by "var". The front contact was assumed to be near ohmic, but the back contact was assumed to form a Schottky barrier, of variable height, with the p-CdTe layer.

Recombination. Recombination centers play two roles in CdS/CdTe cells: (a) energy levels involved in radiative and non-radiative recombination, and (b) charge-density modification by acting as deep donors and acceptors when empty. Since the occupancy of these levels is determined by recombination traffic, it depends on illumination and bias and can thus lead to transients in carrier transport by deforming the energy-band profiles.

Table 1. Parameter values for typical CdTe cell.

	Front Contact	n-CdS	p-CdS_xTe_{1-x}	p-CdTe	Back Contact
Reflection	0.07	—	—	—	0.30
Barrier height (eV)	0.1	—	—	—	0.3, var.
Recomb. velocity, electrons (cm/sec)	10^7	—	—	—	10^7
Recomb. velocity, holes (cm/sec)	10^7	—	—	—	10^7
Thickness (μm)	—	0.1	0.1	2, var.	—
Dielectric coefficient	—	9.0	9.4	9.4	—
Electron affinity	—	4.50	4.28	4.28	—
Band gap (eV)	—	2.42	1.41	1.50	—
Density of states, CB (cm^{-3})	—	$1.8x10^{19}$	$7.5x10^{17}$	$7.5x10^{17}$	—
Density of states, VB (cm^{-3})	—	$2.4x10^{18}$	$1.8x10^{19}$	$1.8x10^{19}$	—
Carrier density (cm^{-3})	—	10^{17}	10^{14}, var.	10^{14}, var.	—
Electron mobility (cm^2/V-sec)	—	350	500	500	—
Hole mobility (cm^2/V-sec)	—	50	60	60	—
Lifetime (sec)	—	10^{-9}	var.	var.	—
Recomb. center density N_r (cm^{-3})	—	10^{15}	var.	var.	—
Recomb. center energy E_r (eV), wrt. VB	—	1.21	0.75	0.75	—
Recomb. cross section σ_n (cm^2)	—	10^{-15}	10^{-12}	10^{-12}	—
Recomb. cross section σ_p (cm^2)	—	10^{-12}	10^{-15}	10^{-15}	—

AMPS calculates recombination rates U using the Shockley-Read-Hall (SRH) formalism, which requires specification of the recombination center density N_r, energy level E_r, and cross sections σ_n and σ_p for each center. N_r and the cross sections enter the SRH equation only in the products $\tau_{no} = 1/N_r v_{th} \sigma_n$ and $\tau_{po} = N_r v_{th} \sigma_p$, where v_{th} is the thermal velocity of the electrons (~ 10^7 cm/sec). The value N_r affects both the charge density (and hence the band shape) and the recombination rate, while σ_n affects only the recombination rate. Thus, for the same values of τ_{no} and τ_{po}, large N_r and small σ values will emphasize the effects of the N_r charge on the band shape, while small N_r and large σ values will minimize the distortion of the bands by N_r charging. The ratio of the cross sections is also important in determining their relative occupancy of centers in that a small ratio of σ_n/σ_p will favor a small occupancy of donor-like levels AMPS has two

modes of operation: (a) the so-called Lifetime mode, in which the recombination is characterized by a lifetime $\tau_n = (n - n_o)/U$ that is assumed to be constant, and (b) the so-called Density of States (DOS) mode (herein renamed the Trap Density TD mode) in which N_r, E_r, σ_n, and σ_p are used to determine τ_n. The latter mode has generally been used in these studies. It is favored because the effective lifetime in portions of the cell that have high generation rates can be strongly affected by carrier traffic in the recombination centers under, and thus τ is a strong function of local carrier densities, whereas N_r, E_r, σ_n, and σ_p are not.

For the TD-mode cases, a capture ratio of $\sigma_n/\sigma_p = 10^3$ for donor-like centers was used, with $\sigma_n = 10^{-12}$ cm^2 for electrons to an empty donor-like center (+) and $\sigma_p = 10^{-15}$ cm^2 for holes to an electron-occupied donor (neutral). These values suggest that N_r is similar in magnitude to the carrier density. Such values will modify the band shapes between light and dark, supporting the experimental observations of transient behavior.

Variation of N_a and Lifetime. Fig. 24 shows calculated band diagrams at zero bias and at maximum-power voltage (V_{max}) for three values of the net acceptor density N_a. Above $N_a = 10^{16}$ cm^{-3} most of the CdTe layer is quasi-neutral and the depletion layers are quite narrow. At 10^{15} cm^{-3} the depletion layers fill most of the CdTe, and for 3 x 10^{13} cm^{-3} and below the electric field is large and constant throughout the CdTe, giving essentially an n/i/p junction. Fig. 25 shows the corresponding plots of the generation (gain) and total recombination (loss) versus distance at V_{max}. For $N_a = 10^{17}$ cm^{-3} a substantial part of the generation is in the field-free quasineutral region where the carriers diffuse readily and recombine in the bulk. For $N_a = 10^{15}$ cm^{-3}, many of the photogenerated electrons face a region of strong reverse field and recombination is highly peaked in this region. For $N_a = 3 \times 10^{13}$ cm^{-3} the electric field is lower and relatively constant so the recombination reflects the generation profile.

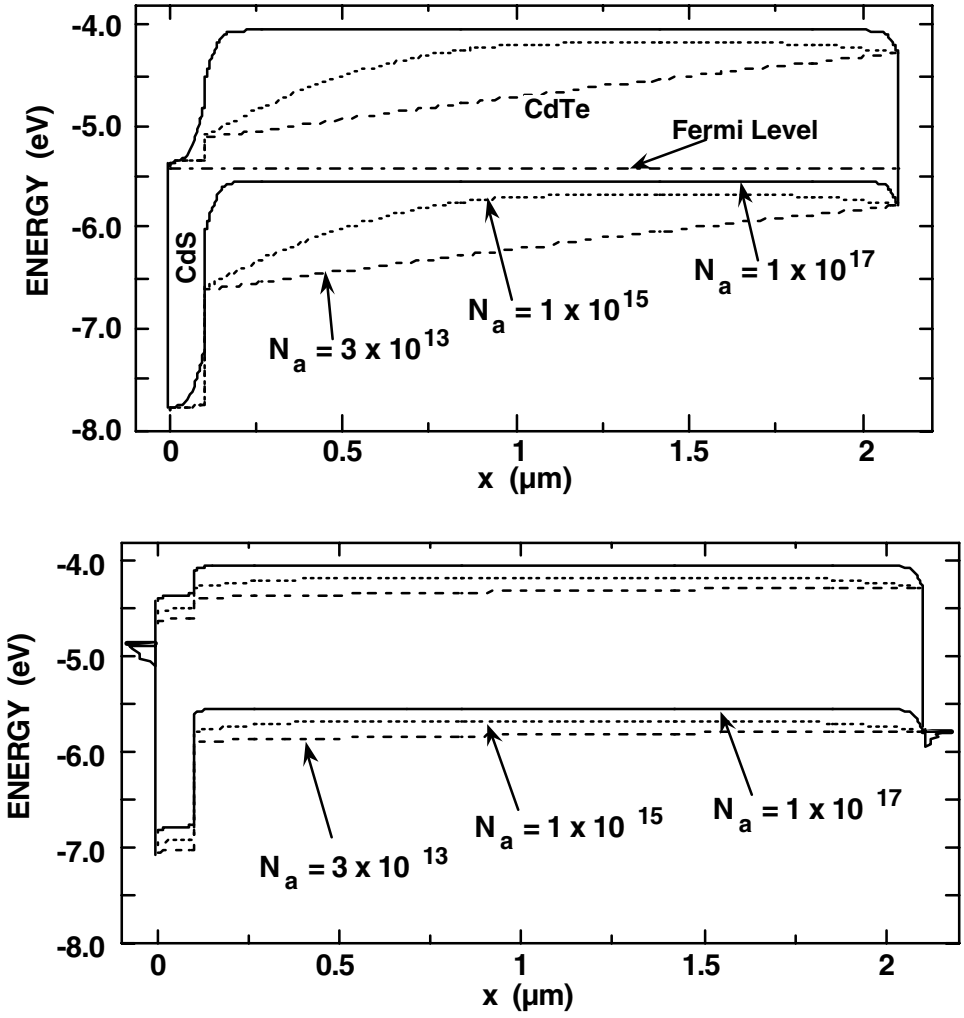

Figure 24. Calculated CdTe band diagrams at zero at the maximum power point. Back barrier is 0.3 eV and $\tau = 10^{-9}$ s.

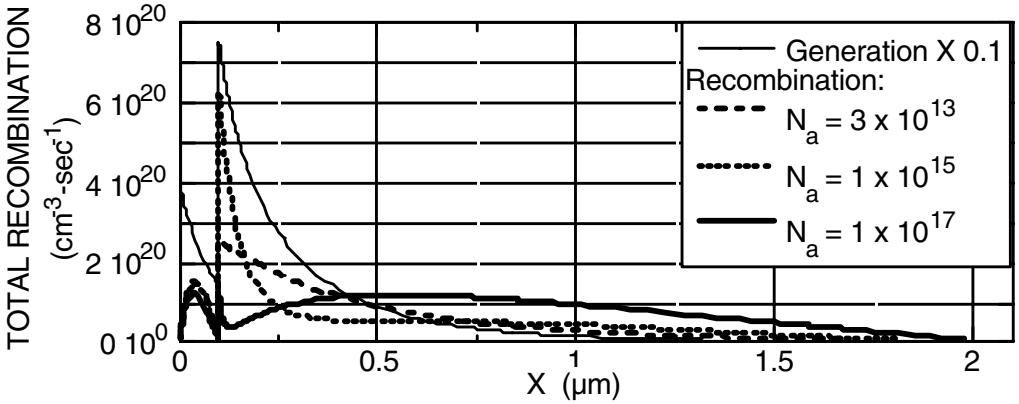

Figure 25. Generation and recombination rates at maximum power.

Fig. 24 shows that the electric field (ε) in the photogeneration region is strongly dependent on N_a. This dependence leads to significant variations in the calculated voltage, current and fill-factor, as shown in Fig. 26.

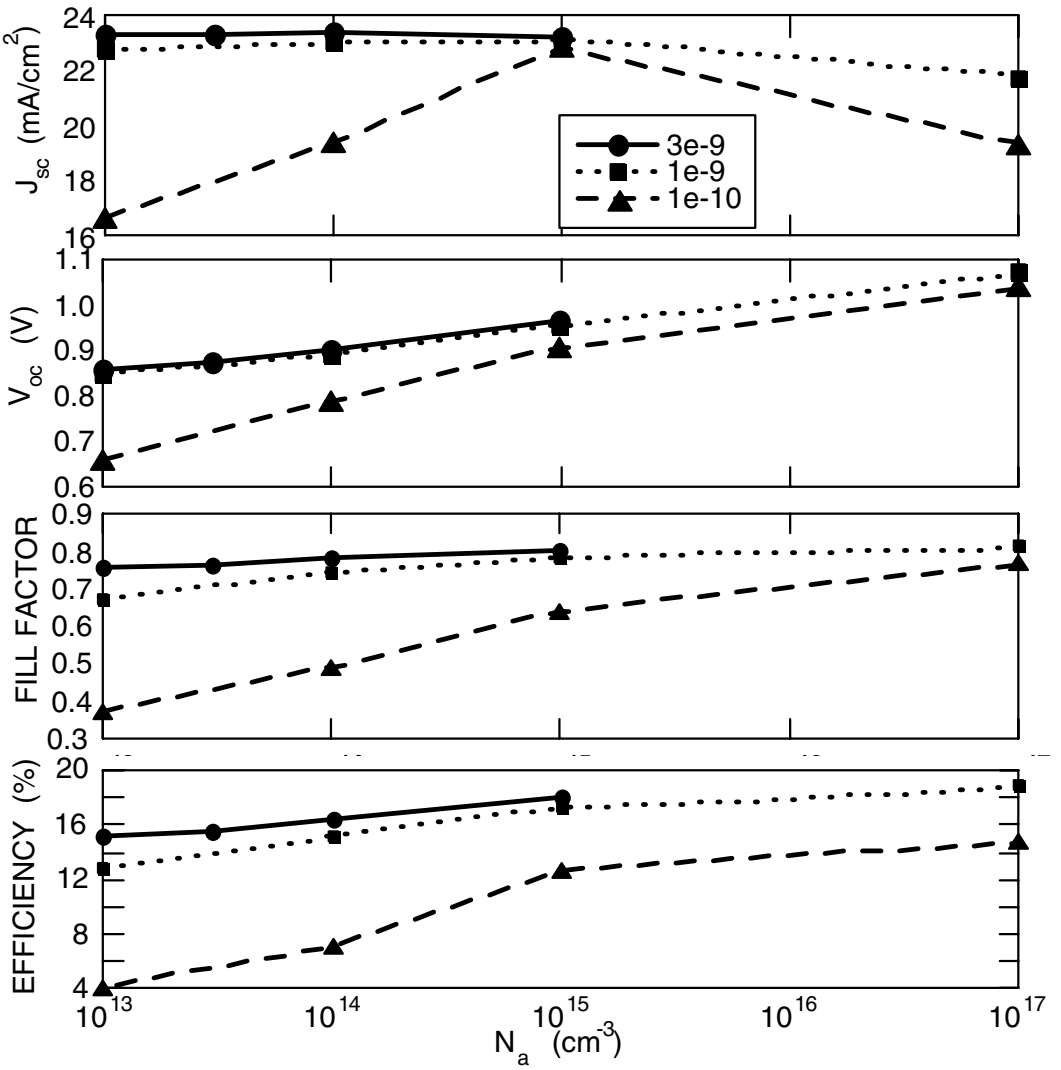

Figure 26. Calculated parameters as a function of carrier density and lifetime.

In the presence of ε, the effective lifetime τ_{eff} is related to the zero-field lifetime τ_o by $\tau_{eff} \sim \tau_o(1 \pm \varepsilon/\varepsilon_c)^2$, where $\varepsilon_c = (kT/\mu\tau)^{0.5}$. The + is for diffusion along the field, and the – is for diffusion against the field [Fahrenbruch and Bube, *Fundamentals of Solar Cells*, Academic Press (1983), p. 83]. For fairly large values of τ_o, as seen in Fig. 26,

variations in τ_{eff} (electric-field-aided collection) have only a small effect on J_{SC}. For smaller values of τ_o, field-aided collection plays a much stronger role. In the region of major generation, the field is largest for $N_a = 2 \times 10^{15}$ cm^{-3}, and J_{sc} shows a maximum. V_{oc} decreases strongly for decreasing N_a, because the potential barrier faced by electrons diffusing across the junction to the right (the bucking current) collapses for smaller N_a. This point will be explored in greater detail below. Series and shunt resistances were not included in the calculation of fill-factor, and hence the trends in Fig. 26 track V_{OC}.

Variation of CdTe Thickness. Examination of variations in CdTe layer thickness yields a number of insights. For these cases, $N_a = 10^{14}$ cm^{-3} and the parameters in Table 1 were assumed, and two extreme cases of back-barrier height were used: $Ø_{bc} = 0$ and 0.5 eV. $Ø_{bc} = 0$ leads to an accumulation region at the back contact that acts as a both an ohmic contact and a minority carrier mirror, a desirable condition, but one not likely achievable in real cells. The results for $Ø_{bc} = 0.5$ eV show the typical anomalies that are seem in the environmental stressing of experimental cells. The band diagrams for these cases are shown in Fig. 27 at zero bias, and the resulting parameters are shown in Fig. 28.

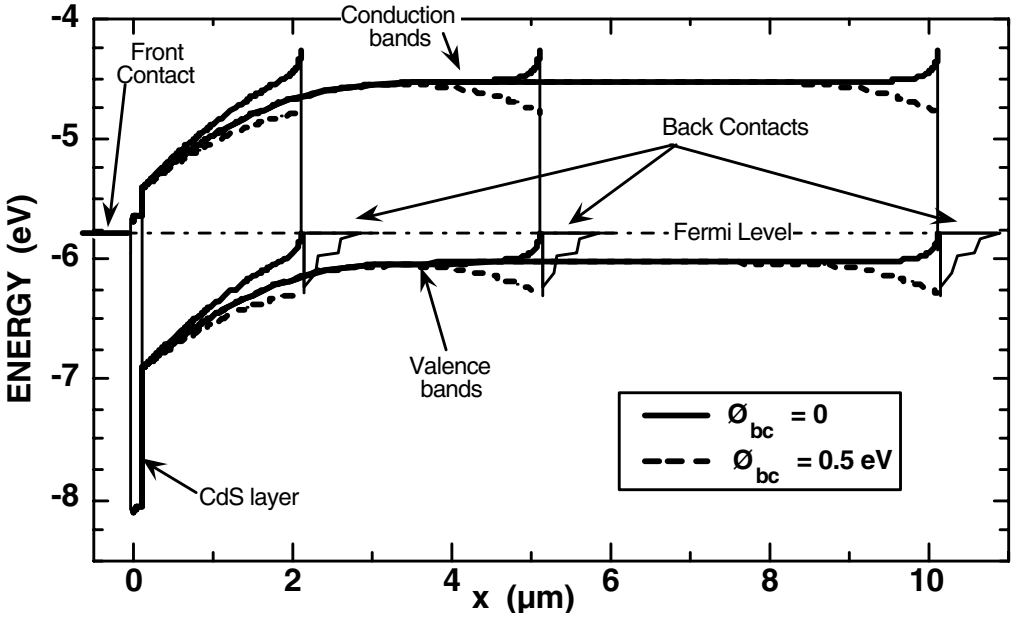

Figure 27. Band diagrams for three CdTe thicknesses and two barrier heights.

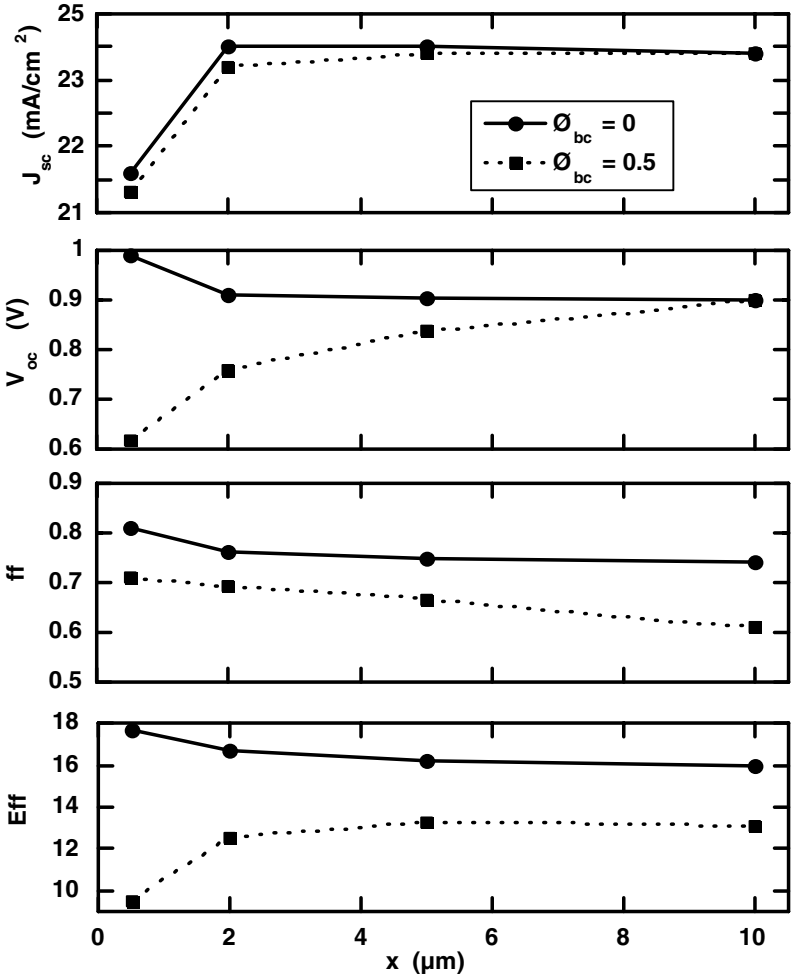

Figure 28. Calculated CdTe parameters as a funtion of thickness.

Fig. 28 shows that J_{sc} is relatively insensitive to $Ø_{bc}$. The decrease in J_{sc} at smaller thicknesses is due to lessening of the absorption volume. For a CdTe thickness of 0.5 μm, almost identical J_{sc} and similar ff values for both $Ø_{bc}$ = 0 and 0.5 eV are obtained, but V_{oc} varies by almost 0.4 eV. The $Ø_{bc}$ = 0.5 eV barrier does not primarily block photogenerated holes, but decreases the effective junction barrier of the cell. Light and dark curves do not cross for $Ø_{bc}$ = 0 and only at very high currents for $Ø_{bc}$ = 0.5 eV.

For $Ø_{bc}$ = 0, V_{oc} becomes larger for thinner CdTe, because the recombination volume becomes smaller and the accumulation layer at the back contact reduces the surface

recombination to very small values. For $Ø_{bc}$ = 0.5 eV, however, V_{oc} is strongly reduced for thinner cells, because the barrier to transport of electrons to the right (bucking current) collapses between 2 μm and 5 μm. In these cases, the reverse field at the back is lessened or nonexistent, and there is no barrier to photogenerated holes, which in turn strongly increases recombination loss at the back contact.

For $Ø_{bc}$ = 0.5 eV, the loss current through bulk recombination in the 2 μm CdTe case is a factor of 2 smaller than that of the 5 μm CdTe due to the smaller recombination volume. However, the surface recombination loss at the back contact is larger by a factor of 7 for the 2-μm cells. Thus the reverse field at the back essentially turns the back surface recombination on or off. For $Ø_{bc}$ = 0, the fill-factor follows the variation of V_{oc}, as expected. However, for $Ø_{bc}$ = 0.5 eV, the fill-factor increases for thinner CdTe layers because the collapse of the barrier changes the character of the back contact, making it ohmic for photogenerated holes traveling to the right.

Since the depletion layer widths depend on N_a, the observed changes take place for thicker (thinner) CdTe layers for lower (higher) N_a values. Variation of the CdTe layer thickness demonstrates the strong influence of back-contact barrier height, leading to the anomalies (V_{oc} shift, cross-over, and roll-over) that are commonly seen in experimental devices, particularly for stressed devices.

Simulation of J-V Anomolies. Starting from a baseline AMPS case that yields J_{SC} of 24 mA/cm^2, V_{OC} of 850 mV, fill-factor of 75%, efficiency near 16%, and the spectral response of generic CdS/CdTe cells, further modeling was done to explain the J-V characteristic anomalies observed as a result of fabrication variables and stressing [McMahon and Fahrenbruch, PVSC **28**, 539 (2000)]. The cell model used here assumes a CdSTe layer and two CdTe layers, with 4 μm total CdTe thickness. The Trap Density mode is used with $N_r = 3 \times 10^{14}$ cm^{-3}, E_r = 0.75 eV, $\sigma_n = 10^{-12}$ cm^2, and $\sigma_p = 10^{-12}$ cm^2 in the CdSTe and CdTe layers. Four situations are compared: high and low Na, and

high and low $Ø_{bc}$. The J-V curves for these four situations are shown in Fig. 29 and the results are summarized in Table 2.

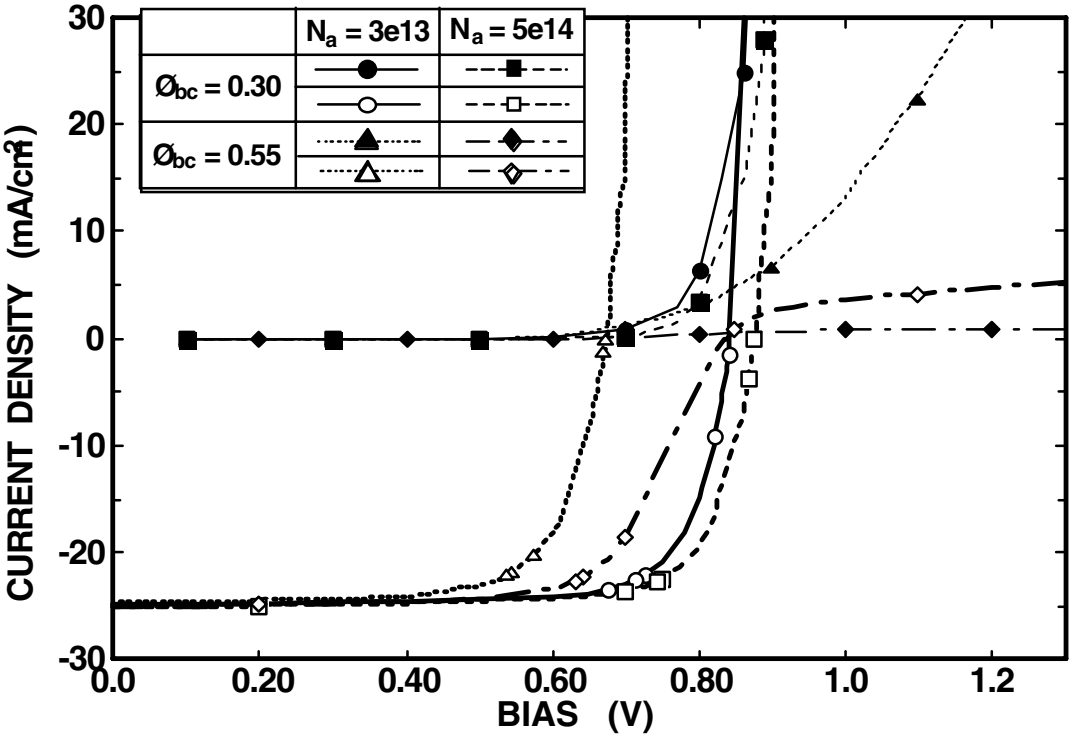

Figure 29. Calculated J-V Characteristics for the four CdTe cases.

Table 2. Summary of J-V characteristic attributes

CASE #	51.1	50.1	51.6	50.6
$Ø_{bc}$	0.30	0.30	0.55	0.55
N_a	3 x 10^{13}	5 x 10^{14}	3 x 10^{13}	5 x 10^{14}
Light Rollover	none	none	some @ > 100 mA	large
Dark Rollover	none	none	some (SCLC)	extreme
Crossover	80 mA	none	severe (@ 0.7 mA)	severe (@ 0.6 mA)
ff	high (0.768)	high (0.768)	fair (0.716)	lowest (0.685)
V_{oc}	high (0.842 V)	highest (0.876 V)	lowest (0.672 V)	High (0.837)
Eff	high (16.1%)	highest (16.8%)	lowest (11.9%)	fair (14.3%)

The relationship of the PV parameters to N_a and $Ø_{bc}$ is shown in more detail in Fig. 30.

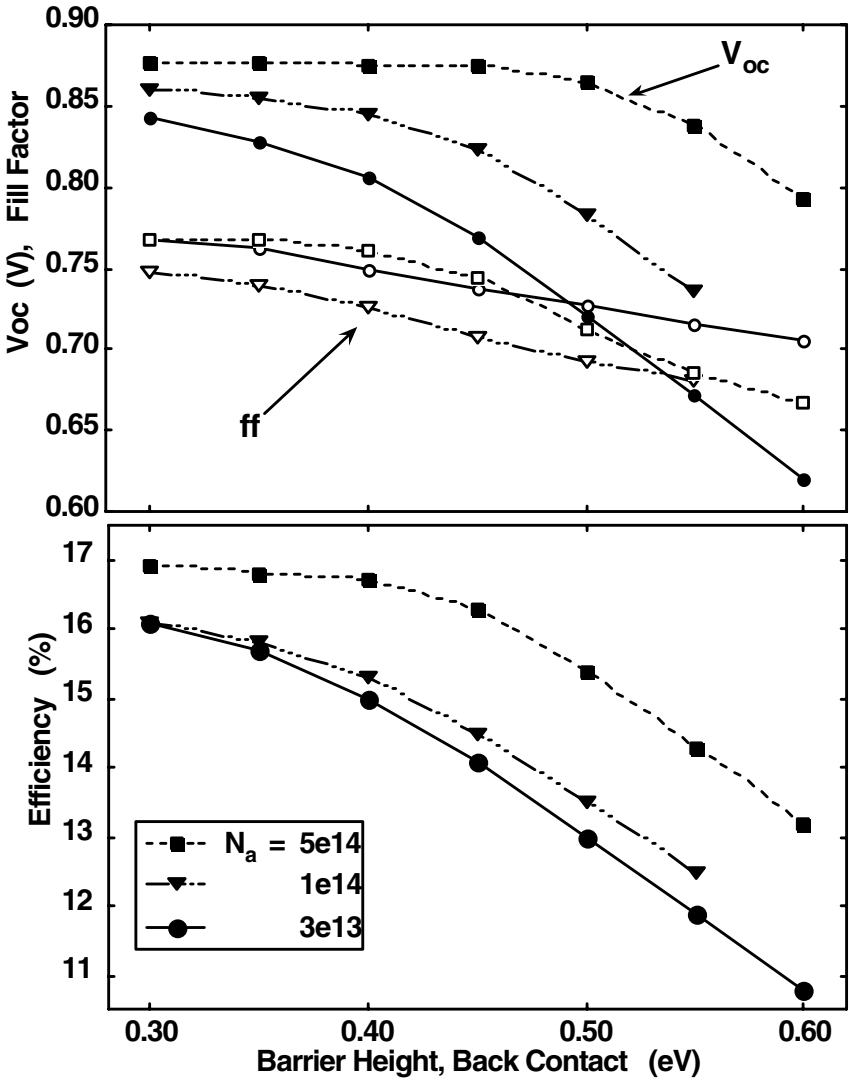

Figure 30. Variation of parameters with back barrier and acceptor density.

To elucidate the causes of these anomalies the band diagrams for the four cases are shown in Fig. 31. Two limiting cases are shown. For zero bias, the influence of back contact is confined to back region of cell with no appreciable influence near junction. Indeed, one might be able to treat the cell as a Schottky barrier in series back-to-back with the main junction. In contrast, the calculated band diagrams in forward bias show a large influence of the back contact that extends throughout cell up to the CdS/CdSTe junction and regulates overall transport. All normal cell operation takes place between these extremes, and the details lead to the different cases summarized in Table 2.

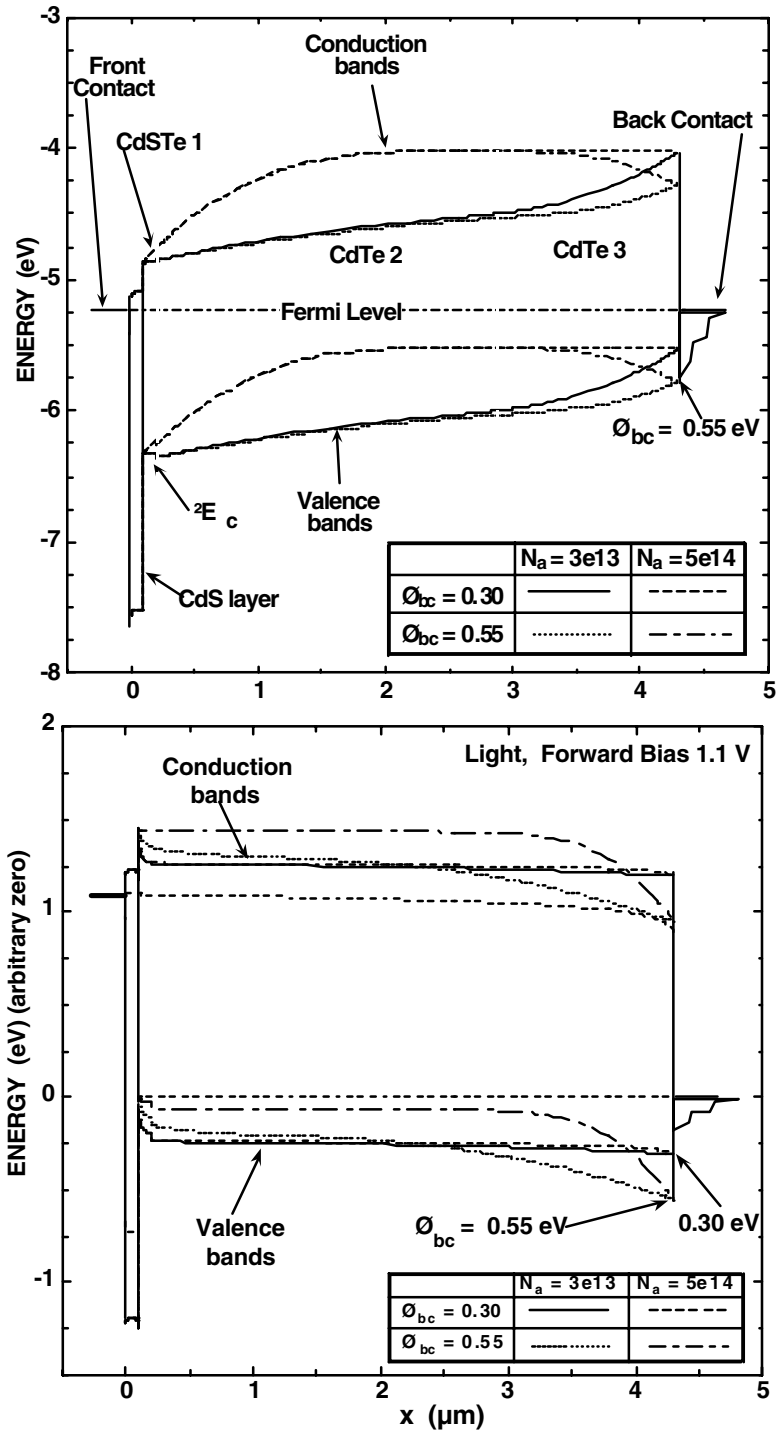

Figure 31. Band diagrams at V = 0 and 1.1 V for the four cases.

The general conclusion from the modeling task is that it is now possible to replicate experimental curves for a significant number of CdTe cells with various features. The

keys to better results have been understanding the consequences of partial overlap of primary and back-contact junctions, the addition of the CdTeS layer to the model, and the proper use of the AMPS trap-density mode. Modeling to date suggests that the largest potential for increased CdTe efficiency is lies in increasing its net acceptor density.

Similar studies on CI(G)S cells are being conducted by Alex Pudov, and are also starting to show results consistent with experimental measurements. Future work will continue to refine CdTe calculations and to bring the CI(G)S calculations up to the same level of understanding and reliability.

CONCLUSIONS AND RECOMMENDATIONS

Whole-cell loss analysis based on precision measurements, careful analytical techniques, and graphical comparisons has been the traditional strength of the Colorado State program, and it continues to show its utility in a number of areas:

(1) Tracking the details of elevated-temperature induced stress in CdTe cells.

(2) Comparisons of CIGS-cell strategies, including replacement of CdS with ZnS, substitution of a partial electrolyte treatment for CdS deposition, sodium inclusion, and precursor electrodeposition vs. physical-vapor deposition.

(3) Understanding of transient behavior found in some CIS cells.

This type of work has been productive and should remain part of the Thin-Film Partnership.

There are also three areas of emerging importance, which have made solid contributions during the subcontract period, and hold the promise of much greater impact:

(1) Micro-nonuniformity studies, used to identify and classify local defects and track changes in them.

(2) Capacitance profiling to elucidate recombination states and their effect on cell performance.

(3) Numerical modeling, especially of CdTe cells, which is becoming considerably more reliable and predictive.

These areas are making the transition from the exploratory to the mainstream and should continue to be refined and extended to additional families of cells.

Finally, the National Team structure has been functioning well for both CdTe and CI(G)S technologies. The collaborative efforts have certainly contributed to our productivity, and they have helped the members accomplish more collectively than likely as individual groups. The recommendation is to maintain the teams as an integral part of the Thin-Film Partnership and explore ways to include our international colleagues.

COMMUNICATIONS

Publications

1. I.L. Eisgruber, J.E. Granata, J.R. Sites, J. Kessler, and J. Hou, "Blue-Photon Modification of Nonstandard Barrier in $CuInSe_2$ Solar Cells," Solar Energy Materials and Solar Cells **53**, 367 (1998).

2. J.R. Sites, J.E. Granata, and J.F. Hiltner, "Losses Due to Polycrystallinity in Thin-Film Solar Cells," Solar Energy Materials and Solar Cells **55**, 43 (1998).

3. JE. Granata and J. R. Sites, "Impact of Sodium in the Bulk and Grain Boundaries of $CuInSe_2$," Proc. 2nd World PV Energy Conf., p. 604 (1998).

4. J.F. Hiltner and J.R. Sites, "Stability of CdTe Solar Cells at Elevated Temperatures: Voltage, Temperature, and Cu Dependence," AIP Conf. Series **462**, 170 (1998).

5. R. Bhattacharya, W. Batchelor, J.F. Hiltner, and J.R. Sites, "Thin-Film $CuIn_{1-x}Ga_xSe_2$ Photovoltaic Cells from Solution-Based Precursor Layers," Appl. Phys. Lett. **75**, 1431 (1999).

6. M.A. Contreras, B. Egaas, K. Ramanathan, J.F. Hiltner, A. Swartzlander, F. Hasoon, and R. Noufi, "Progress Toward 20% Efficiency in $Cu(In,Ga)Se_2$ Polycrystalline Thin-Film Solar Cells," Prog. in Photovoltaics **7**, 311 (1999).

7. J.R. Sites, A.D. Compaan, R.W. Birkmire, C.S. Ferekides, and A.F. Fahrenbruch, "Critical Issues and Research Needs for CdTe Solar Cells," Electrochemical Society Proc. **99-11**, 241 (1999).

8. R.N. Bhattacharya, J.F. Hiltner, W. Batchelor, M.A. Contreras, R. Noufi, and J.R. Sites, "15.4% $CuIn_{1-x}Ga_xSe_2$-Based Solar Cells from Solution-Based Precursor Films," Thin Solid Films **361-362**, 396 (2000).

9. J.F. Hiltner and J.R. Sites, "High-Resolution Laser Stepping Measurements on Polycrystalline Solar Cells," Proc. 16th European PV Solar Energy Conf., p. 630 (2000).

10. S.E. Asher, F.S. Hasoon, T.A. Gessert, M.R. Young, P. Sheldon, J.F. Hiltner, and J.R. Sites, "Determination of Cu in CdTe/CdS Devices Before and After Accelerated Stress Testing," Proc. 28th IEEE PV Specialists Conf., p. 479 (2000).

11. J.F. Hiltner and J.R. Sites, "Local Photocurrent and Resistivity Measurements with Micron Resolution," Proc. 28th IEEE PV Specialists Conf, p. 543 (2000).

12. P. Johnson, J. Sites, K. Ramanathan, L. Olsen, and D. Tarrant, "Effects of Buffer Layers on SSI GIGSS-Absorber Transient I-V and C-V Behavior," Proc. 28th IEEE PV Specialists Conf. p. 618 (2000).

13. J.F. Hiltner and J.R. Sites, "Micron-Resolution Photocurrent of CdTe Solar Cells Using Multiple Wavelengths," Mat. Res. Soc. Proc. **668**, H9.8 (2001).

14. P.K. Johnson, J.R. Sites, and D. Tarrant, "Investigation of the Trapping Mechanism for Transient Current-Voltage Behavior in CIGSS-Based Solar Cells," Mat. Res. Soc. Proc. **668**, H5.12 (2001).

15. J.R. Sites, "Quantification of Losses in Thin-Film Polycrystalline Solar Cells," Proc. PVSEC-12, p. 627 (2001) and Solar Energy Materials and Solar Cells, in press.

16. K. Ramanathan, F.S. Hasoon, H. Al-Thani, P.K. Johnson, and J.R. Sites, "Effect of Cd Solution Treatment of the Photovoltaic Properties of $CuInGaSe_2$ Thin-Film Junctions," submitted to Appl. Phys. Lett.

Presentations

1. J.R. Sites, "Transients in SSI Cells," CIS Team Meeting, Golden, April 1998.

2. J.E. Granata, "Reverse-Bias Breakdown in NREL CIGS Cells," CIS Team Meeting, Golden, April, 1998.

3. J..F. Hiltner, "Stress Testing at CSU", CdTe Team Meeting, Denver, September 1998.

4. J.F. Hiltner, "High Resolution Laser Stepping Apparatus," CIS Team Meeting, Tampa, February 1999.

5. J.R. Sites, "Critical Issues for CdTe Solar Cells," ECS Meeting, Seattle, May 1999.

6. P.K. Johnson, "Cell Characterization," APS Regional Meeting, Tucson, October 1999.

7. J.F. Hiltner, "Laser-Stepping Measurements of GSI CIGS Cells," CIS Team Meeting, Golden, October 1999.

8. J.R. Sites, "CdTe Cells: How Does One Demonstrate 30-Year Stability?" CdTe Team Meeting, Golden, January 2000.

9. J.R. Sites, "The National CdTe and CIS R&D Teams," NCPV Review Meeting, Denver, April 2000.

10. J.R. Sites (with R.W. Birkmire), *Thin-Film Tutorial*, Anchorage, September 2000.

11. J.F. Hiltner, "Local Photocurrent Measurments", PVSC Conf., Anchorage, September 2000.

12. J.R. Sites, "What's New With Solar Cells?" Gustavus Adolphus and St. Olaf's Colleges, November 2000; Metro State College, February 2001.

13. J.F. Hiltner, "Micron-Resolution Photocurrent," MRS, San Francisco, April 2001.

14. J.R. Sites, "Thin-Film Polycrystalline Cells," Seoul National University and Mokpo University, Korea, June 2001.

15. J.R. Sites, "Loss Analysis," PVSEC-12, Che Ju Island, Korea, June 2001.

Graduate Degrees

1. Jason Hiltner (M.S., May 1998) Coursework/Research Project

2. Jennifer Granata (Ph.D., December 1998) Thesis: "The Impact of Deliberate Sodium Incorporation on $CuInSe_2$-Based Solar Cells"

3. Pamela Johnson (M.S., May 1999) Coursework/Research Project

4. Jason Hiltner (Ph.D., May 2001) Thesis: "Investigation of Spatial Variations in Collection Efficiency of Solar Cells" www.colostate.edu/orgs/pvlab

5. Alexei Pudov (M.S., August 2001) Coursework/Computational Project

Specific Reports

Date	To Lab/Person	Done By	Topic
5/28/98	ISET/Basol	Johnson	CIS loss analysis
7/29/98	Global Solar/Wendt	Granata	ITO optical measurements
8/21/98	Siemens/Tarrant	Johnson	CIS after light and dark cycles
9/7/98	CdTe Team	Hiltner	CdTe stress tests
9/23/98	ISET/Basol	Granata	ZnO optical measurements
11/2/98	NREL/Ramanathan	Granata	CdS vs. Zn-PE treatment of CIGS
11/5/98	NREL/CdTe Group	Hiltner	CdTe stress with standard contacts

11/7/98	ANTEC/Bonnet	Hiltner	CdTe stress with ANTEC contacts
11/9/98	NREL/CdTe Group	Hiltner	CdTe stress with varied contacts
12/2/98	Siemens/Tarrant	Granata	CIS after dark and light cycles
12/17/98	NREL/Bhattacharya	Hiltner	Electrodeposited CIS cells
1/25/99	NREL/Contreras	Hiltner	Analysis of record CIGS cell
2/12/99	ISET/Basol	Hiltner	Cu- vs. In(Ga)-rich CIGS cells
2/16/99	Wash. State/Olsen	Hiltner	CdS vs. non-CdS CIS cells
3/16/99	Internal	Fahrenbruch	AMPS modeling of CdTe cells
4/22/99	Seimens/Tarrant	Hiltner et al	Transient effects with SSI absorbers
6/7/99	NREL/Ramanathan	Johnson	Cells with thin CIGS absorber
6/21/99	NREL/Ramanathan	Johnson	Temperature variations in CdS growth
7/26/99	Unisun/Eberspacher	Johnson	CIS loss analysis
8/2/99	Internal	Macedo	Characterization of light sources
8/6/99	General	Hiltner	Small-spot laser stepping apparatus
8/15/99	First Solar/Rose	Pudov	CdTe stress: long-term recovery
8/16/99	NREL/Albin	Macedo	CdTe stress vs. temperature
9/8/99	ISET/Leidholm	Hiltner	CIS loss analysis
9/13/99	ITN and NREL	Johnson	CdTe cells with varying ITO
9/29/99	Global Solar/Britt	Hiltner	Small CIS features
10/1/99	CIS Transient Team	Sites	Summary of Siemens transients
10/22/99	NREL/Wu	Johnson	CdTe stress tests
10/25/99	First Solar/Rose	Hiltner	Optical losses
10/29/99	A. Gakuin/Nakada	Sites	CIGS loss analysis
11/29/99	NREL/Wu	Johnson	CdTe stress tests
12/8/99	IEC/McCandless	Hiltner	Small CdTe features
12/9/99	NREL/Wu	Sites	CdTe stress tests
1/28/00	CdTe Team	Fahrenbruch	Transport modeling in CdTe cells
2/3/00	NREL/Contreras	Hiltner	CIGS variations with CdS thickness
3/14/00	CIS Transient Team	Johnson	Transients in SSI/WSU/IEC CIS cells
4/6/00	FSEC/Dhere	Johnson	Loss analysis of $Cu(In,Ga)S_2$ cells

5/5/00	CIS Transient Team	Johnson	Transients in SSI/NREL CIS cells
6/9/00	CIS Transient Team	Johnson	Contrast of NREL and SSI transients
7/1/00	Internal	Fahrenbruch	Modeling of CdS/CdTe cells
7/15/00	Internal	Pudov	AMPS baseline for GIGS
8/11/00	IEC/Shafarman	Pudov	Transients in IEC CIGS cells
8/15/00	Internal	Glöckler	Data tracking of 50-W panel/battery
10/17/00	CIS Transient Team	Johnson	Comparison of transients
11/27/00	ISET/Le	Johnson	CIS loss analysis
1/16/01	First Solar/Rose	Hiltner	Stress effect on CdTe microstructure
1/25/01	CdTe Team	Sites	Proposed model for CdTe changes
1/26/01	CdTe Team	Fahrenbruch	Effect of CdTe back barrier
2/15/01	CSU/Sampath	Jenkins	Loss analysis of CdTe cells
5/18/01	A. Gakuin/Nakada	Pudov	Loss analysis of ZnS/CIGS cells
8/21/01	Internal	Demtsu	Calibration of light sources
8/24/01	NREL/Wu	Jenkins	Loss analysis of CdTe cells
9/15/01	CSU/Sampath	Demtsu	Loss analysis of CdTe cells
9/26/01	FSEC/Dhere	Glöckler	Loss analysis of $Cu(In,Ga)S_2$ cells